International Journal of Non-Linear Mechanics 118 (2020) 103290

Contents lists available at ScienceDirect

International Journal of Non-Linear Mechanics

journal homepage: www.elsevier.com/locate/nlm

A nonlinear model for a hanging cantilevered pipe discharging fluid with a partially-confined external flow

A.R. Abdelbaki[1], M.P. Païdoussis *, A.K. Misra

Department of Mechanical Engineering, McGill University, 817 Sherbroke Street West, Montreal, QC, Canada H3A 0C3

ARTICLE INFO

Keywords:
Hanging cantilevered pipes
Axial flows
Pipe conveying fluid
Nonlinear dynamics

ABSTRACT

In this paper, a nonlinear theoretical model is developed for the dynamics of a flexible cantilevered pipe that is simultaneously subjected to internal and partially-confined external axial flows. The pipe under consideration discharges fluid downwards, which accumulates in a relatively large tank, and then flows upwards through a generally shorter annular region surrounding the pipe. Thus, the internal and external flows are interdependent and in opposite directions. A practical application of this system may be found in solution mining processes for brine production, and in the subsequent usage of the salt-mined caverns for hydrocarbon storage. The equation of motion is derived using the extended Hamilton's principle to third-order accuracy with a separate derivation of the fluid-related forces associated with the internal and external flows. The equation is discretized using Galerkin's scheme and solved via the pseudo-arclength continuation method and a direct time integration technique. Two pipes of different dimensions and materials are considered in this study; the stability of these pipes is investigated with increasing flow velocity. Also, the influence of varying the length and tightness of the annular region on the dynamical behaviour of the pipes is explored theoretically. The predictions of the proposed model are compared to experimental observations from the literature for systems with the same parameters as those considered in this paper, as well as to predictions of an earlier linear theory. The results obtained are in excellent qualitative and good quantitative agreement with the experimental observations. Furthermore, this model predicts the frequencies of oscillation more accurately than linear theory.

1. Introduction

Systems that involve flexible pipes subjected to simultaneous internal and external axial flows are very common in industry; e.g., they can be found in heat exchangers, drill strings used in drilling operations and oil exploration, and brine strings used for brine production. Cesari and Curioni [1] were the first to investigate the static stability of such a system with different boundary conditions. Pipes subjected to concurrent internal and external axial flows were studied theoretically afterwards by Hannoyer and Païdoussis [2]; this work was extended by Païdoussis and Besançon [3] who considered arrays of cylinders with internal and external flows. Wang and Bloom [4] examined the dynamics of an inclined pipe subjected to internal and partially-confined external flows; they formulated a linearized mathematical model to determine the system eigenfrequencies, and identified the critical parameters pertaining to stability of the system.

Païdoussis et al. [5] derived a linear theoretical model for a vertical cantilevered pipe discharging fluid downwards, which then flows upwards through an annular region contained by a rigid channel; thus, the internal and external flows are interdependent and the external flow is fully confined; i.e., confined over the whole length of the pipe. Two sets of system parameters were considered: the first one corresponds to a bench-top-size system, while the second idealizes a drill-string-like system. It was concluded in [5] that if the degree of confinement of the external flow is sufficiently high, the external flow is dominant and it destabilizes the system. A nonlinear model for that particular configuration was developed by Abdelbaki et al. [6,7] and the results obtained were compared to the theoretical results of [5] and experimental observations by Rinaldi [8]; the model successfully captures the essentials of the behaviour observed experimentally. The effects of reversing the flow direction on the dynamical behaviour of the system in [5] were explored theoretically by Qian et al. [9] who assumed that the hanging pipe is aspirating the fluid in a simple manner. Recently, Fujita and Moriasa [10] revisited the theoretical modelling of the same system, considering the two different directions of the flow velocities [5,9]; they employed the principle of superposition of linear stability analysis of a pipe subjected to internal and external flows separately to examine the dynamics of the system. Later on, Zhao et al. [11] modelled the drill-string as a stepped pipe to take into account the differences between the drill-pipe and the drill-collar

* Corresponding author.
E-mail address: michael.paidoussis@mcgill.ca (M.P. Païdoussis).
[1] On Leave from Mechanical Design and Production Dept., Faculty of Engineering, Cairo University, Giza 12613, Egypt.

https://doi.org/10.1016/j.ijnonlinmec.2019.103290
Received 1 May 2019; Received in revised form 6 September 2019; Accepted 26 September 2019
Available online 28 September 2019

diameters; they developed a linear model and explored the influence of various parameters on the stability of the system.

Moditis et al. [12] studied the dynamics of a discharging cantilever pipe with reverse, partially-confined, external flow — a system that models one of the *modi operandi* of salt-mined caverns used for storage and subsequent retrieval of hydrocarbons [13]. Moditis et al. extended the theoretical model of [5] and derived a linear equation of motion for the pipe. The theoretical analysis was validated by comparison with experiments in a bench-top-sized system in the same study. In addition, the linear theory was used to investigate the stability of long brine-string-like systems [12]; it was found that sufficiently long systems lose stability with increasing flow velocity via divergence rather than flutter, the latter being the mode of instability observed experimentally in the bench-top-sized system. The same configuration was studied numerically by Kontzialis et al. [14]; the results obtained were in a good agreement with the experiments in [12].

Moreover, Minas et al. [15] investigated the effect of adding an end-piece at the free end of the pipe that makes the flow to be discharged radially instead of axially as in [12,14]; this idea was originally explored by Rinaldi and Païdoussis [16] experimentally and theoretically, but for a cantilevered pipe discharging fluid without any external flow. It was concluded in [15] that discharging the flow radially stabilizes the system against flutter, the same conclusion reached earlier in [16].

Most recently, Abdelbaki et al. [17] improved the theory in Moditis et al. [12] by modelling the external flow in a more accurate and realistic manner, and thus obtained a better prediction for the thresholds of instability and the associated frequencies of oscillation, especially for longer annular regions.

In the present study, the nonlinear dynamics of a hanging cantilevered pipe simultaneously subjected to internal and *partially-confined* external axial flows is examined by a nonlinear theory for the first time. The nonlinear equation of motion is derived to third-order accuracy in Section 2. In Section 3, the new theoretical model is used to investigate the stability of two pipes of different dimensions and materials, and with different lengths of the annular region. In Section 4, the critical flow velocities for instability, as well as the amplitudes and frequencies of oscillation at various flow velocities, obtained using the proposed model, are compared to the experimental data reported in [12] for systems with parameters similar to those considered in Section 3. The influence of varying the tightness of the annular region on the stability of the system is investigated theoretically in Section 5.

2. Derivation of the theoretical model

A long flexible cantilevered pipe such as shown in Fig. 1a is considered, with outer diameter D_o, inner diameter D_i, length L, flexural rigidity EI and mass per unit length m. The pipe conveys a fluid downwards with a uniform flow velocity U_i, discharging it into a relatively large tank filled with the same fluid. The fluid then flows upwards with velocity U_o through an annular region contained by a rigid tube of internal diameter D_{ch} and length L', exiting at $X = 0$. The system is oriented vertically, and the neutral axis of the pipe coincides with the X-axis and the gravity direction, $\vec{g}$, as shown in Fig. 1a.

The main assumptions made for the system can be listed as follows: (i) the pipe length-to-diameter ratio is high, so it can be modelled via Euler–Bernoulli beam theory; (ii) the centreline of the pipe is assumed to be inextensible; (iii) the pipe may undergo large deformation, but the strains remain small; (iv) the motion of the pipe is assumed to be planar, i.e. in the (X, Y)-plane, and thus the derived model is two-dimensional; (v) the fluid is incompressible; (vi) the tank size is assumed to be large; therefore, the external flow velocity is assumed to have a value of U_o in the confined region only, while $U_o = 0$ over the unconfined one; and lastly (vii) the internal flow velocity, U_i, and the external one in the confined region, U_o, are assumed to be uniform, and they are related to each other according to the law of conservation of mass.

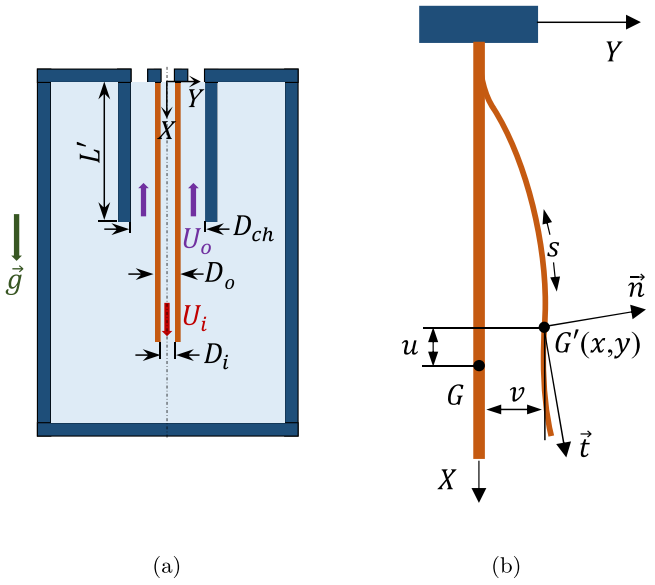

Fig. 1. (a) Diagram of a vertical hanging pipe discharging fluid downwards, which then flows upwards through an annular region surrounding the pipe. (b) Diagram defining the coordinate systems used, and the displacements of point G on the neutral axis of the pipe, located at $G(X, 0)$ before deformation and at $G'(x, y)$ after deformation.

In the following analysis, the Lagrangian coordinate system (X, Y, Z, t) is used to describe the undeformed state of the pipe, while the Eulerian one (x, y, z, t) is associated with the deformed state. Thus, the displacements of a point, say G, on the centreline of the pipe, due to deformation may be determined by $u = x - X$, $v = y - Y$, and $w = z - Z$ — see Fig. 1b. In addition, one can write $Y = 0$, $v = y$ and $z = Z = w = 0$, because the pipe is assumed to move only in the (X, Y)-plane. The curvilinear coordinate along the pipe, s, can be used instead of X, where $\partial s/\partial X = 1 + \bar{\varepsilon}$ and $\bar{\varepsilon}$ is the axial strain along the pipe centreline; since the pipe is assumed to be inextensible, $\bar{\varepsilon} = 0$, $\partial s/\partial X = 1$. Also, from the relation $1 + \bar{\varepsilon}(X) = [(\partial x/\partial X)^2 + (\partial y/\partial X)^2]^{1/2}$, one can derive the following inextensibility condition $(\partial x/\partial X)^2 + (\partial y/\partial X)^2 = 1$, and thus obtain the curvature, $\bar{\kappa}$, along the deformed pipe,

$$\bar{\kappa} = \frac{\partial^2 y/\partial s^2}{\sqrt{1 - (\partial y/\partial s)^2}}. \tag{1}$$

The reader is referred to [18] for detailed derivations.

The equation of motion is derived via the extended Hamilton's principle,

$$\delta \int_{t_1}^{t_2} \mathcal{L}\, \mathrm{d}t + \int_{t_1}^{t_2} \delta W\, \mathrm{d}t = 0, \tag{2}$$

where $\mathcal{L}$ is the Lagrangian and δW is the total virtual work done on the pipe. The Lagrangian is expressed as $\mathcal{L} = \mathcal{T} - \mathcal{V}$, where $\mathcal{T}$ is the kinetic energy of the pipe including the conveyed fluid, and $\mathcal{V}$ is the associated potential energy. Also, the total virtual work $\delta W = \delta W_i + \delta W_o$ consists of: δW_i, the virtual work due to the fluid forces related to the internal flow but not included in the Lagrangian, and δW_o, associated with the external flow. The theoretical model derived in the present study is exact to third-order of magnitude, $\mathcal{O}(\epsilon^3)$, for $y = v \sim \mathcal{O}(\epsilon)$ and $u \sim \mathcal{O}(\epsilon^2)$. Hence, all the expressions derived for the virtual work must be correct to $\mathcal{O}(\epsilon^3)$, and all the energy expressions to $\mathcal{O}(\epsilon^4)$.

2.1. Total kinetic and potential energies of the pipe including the conveyed fluid

The nonlinear expressions for the kinetic and potential energies of a pipe conveying fluid were derived in detail by Semler et al. [18]; the same expressions can be used for the configuration under study. The

total kinetic energy, $\mathcal{T}$, is the sum of the kinetic energy of the pipe $\mathcal{T}_p$ and the kinetic energy of the internal fluid $\mathcal{T}_f$; it can be written as follows:

$$\mathcal{T} = \mathcal{T}_p + \mathcal{T}_f = \frac{1}{2}m\int_0^L V_p^2 \mathrm{d}X + \frac{1}{2}M_i\int_0^L V_f^2 \mathrm{d}X, \tag{3}$$

where $\vec{V}_p = \dot{x}\vec{i}+\dot{y}\vec{j}$ is the velocity of a pipe element, with the unit vectors $\vec{i}$ and $\vec{j}$ representing the axial and lateral directions of the undeformed state of the pipe, respectively. M_i is the mass of the fluid per unit length of the pipe, and $\vec{V}_f = \vec{V}_p + U_i\vec{t}$ is the velocity of a fluid element, with the unit vector $\vec{t}$ representing the tangential direction along s, as indicated in Fig. 1b. Thus, from the inextensibility condition, one can write $\vec{t} = (\partial x/\partial s)\vec{i} + (\partial y/\partial s)\vec{j}$, and consequently, $\vec{V}_f = [(\partial/\partial t) + U_i(\partial/\partial s)](x\vec{i} + y\vec{j})$. Substitution of V_p and V_f in Eq. (3) yields the following expression: $\mathcal{T} = (m/2)\int_0^L(\dot{x}^2 + \dot{y}^2)\mathrm{d}s + (M_i/2)\int_0^L[(\dot{x} + Ux')^2 + (\dot{y} + Uy')^2]\mathrm{d}s$, with $(\,)' = \partial(\,)/\partial s$ and $\dot{(\,)} = \partial(\,)/\partial t$. By applying the variational technique and keeping in mind the orders of magnitude, the following relation can be obtained — see [18,19]:

$$\begin{aligned}\delta\int_{t_1}^{t_2}\mathcal{T}\,\mathrm{d}t = &-\int_{t_1}^{t_2}\int_0^L[(m+M_i)\ddot{x} + 2M_iU_i\dot{x}']\delta x\,\mathrm{d}s\,\mathrm{d}t\\ &-\int_{t_1}^{t_2}\int_0^L[(m+M_i)\ddot{y} + 2M_iU_i\dot{y}']\delta y\,\mathrm{d}s\,\mathrm{d}t\\ &+M_iU_i\int_{t_1}^{t_2}[\dot{x}_{\,L}\delta x_{\,L} + \dot{y}_{\,L}\delta y_{\,L}]\,\mathrm{d}t,\end{aligned} \tag{4}$$

where $x_{\,L} = x(L)$ and $y_{\,L} = y(L)$ are the displacements of the free end of the pipe.

Similarly, the total potential energy, $\mathcal{V}$, is determined by summation of the strain and gravitational energies of the pipe itself, as well as the gravitational energy of the fluid. Thus, one can write

$$\mathcal{V} = \frac{1}{2}EI\int_0^L \bar{\kappa}^2\,\mathrm{d}X - (m+M_i)g\int_0^L x\,\mathrm{d}X. \tag{5}$$

Utilizing the curvature expression (1) and applying the variational technique leads to

$$\begin{aligned}\delta\int_{t_1}^{t_2}\mathcal{V}\,\mathrm{d}t = &EI\int_{t_1}^{t_2}\int_0^L[y'''' + 4y'y''y''' + y''^3 + y''''y'^2]\,\delta y\,\mathrm{d}s\,\mathrm{d}t\\ &-(m+M_i)g\int_{t_1}^{t_2}\int_0^L[-(y' + \frac{1}{2}y'^3)\\ &+(L-s)(y'' + \frac{3}{2}y''y'^2)]\,\delta y\,\mathrm{d}s\,\mathrm{d}t + \mathcal{O}(\epsilon^5).\end{aligned} \tag{6}$$

It should be noted that the relation between δx and δy can be obtained by applying the variational operator, δ, to the inextensibility condition, eventually yielding

$$\delta x = -(y' + \frac{1}{2}y'^3)\delta y + \int_0^s (y'' + \frac{3}{2}y'^2y'')\delta y\,\mathrm{d}s. \tag{7}$$

2.2. Virtual work due to the internal-fluid-related forces

It was shown in [18] that the virtual work, δW_i, is non-zero even if there are no explicit external forces applied on the pipe. This is because of the existence of non-conservative forces associated with the discharging fluid at the free end of the pipe, as originally shown by Benjamin [20]; these forces are not included in the expression of the Lagrangian. According to [18], one can express the virtual work associated with these forces as follows:

$$\delta W_i = -M_iU_i\left(\frac{\partial\vec{r}_{\,L}}{\partial t} + U_i\vec{t}_{\,L}\right).\delta\vec{r}_{\,L}, \tag{8}$$

where $\vec{r}_{\,L}$ represents the position unit vector $\vec{r} = (x, y)$ at the free end of the pipe, and $\vec{t}_{\,L}$ the tangential one at the same position. Eq. (8) leads to

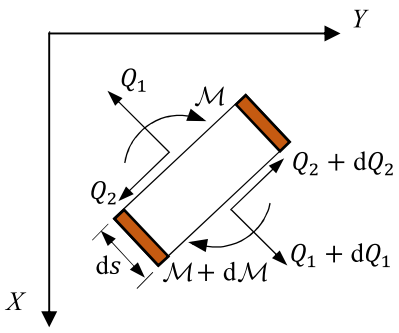

Fig. 2. Free-body diagram of an element of the cantilevered pipe considering the effects of only the internal flow.

$$\begin{aligned}\int_{t_1}^{t_2}\delta W_i\,\mathrm{d}t &= -M_iU_i\int_{t_1}^{t_2}[(\dot{x}_{\,L} + U_ix'_{\,L})\delta x_{\,L} + (\dot{y}_{\,L} + U_iy'_{\,L})\delta y_{\,L}]\,\mathrm{d}t\\ &= -M_iU_i\int_{t_1}^{t_2}(\dot{x}_{\,L}\delta x_{\,L} + \dot{y}_{\,L}\delta y_{\,L})\,\mathrm{d}t - M_iU_i^2\\ &\quad\times\int_{t_1}^{t_2}(x'_{\,L}\delta x_{\,L} + y'_{\,L}\delta y_{\,L})\,\mathrm{d}t\\ &= A + B.\end{aligned} \tag{9}$$

Term A cancels the last term in Eq. (4) and, by employing the inextensibility condition, the following expression for term B can be obtained, with the aid of Eq. (7):

$$B = -M_iU_i^2\int_{t_1}^{t_2}\int_0^s\left[y'' + y'^2y'' - y''\int_s^L(y'y'')\,\mathrm{d}s\right]\delta y\,\mathrm{d}s\,\mathrm{d}t. \tag{10}$$

The analysis presented so far follows exactly that provided in [18] for a hanging cantilevered pipe conveying fluid. Therefore, substituting the expressions obtained for the virtual work and the Lagrangian in the extended Hamilton's principle (2) leads to the final equation of motion derived in [18]. However, the pipe in [18] is assumed to be unconfined and to discharge the fluid to atmosphere, while in the problem in hand, the pipe is simultaneously subjected to an external flow, and the pipe is discharging the fluid into a tank that is filled with the same fluid. Thus, pressurization at the free end of the pipe is important, and should be taken into account. In the following sub-section, the effects of pressurization and externally applied tension at the free end of the pipe are incorporated in the model.

2.3. Pressurization at the free end of the pipe

An element of the pipe of length δs that is subjected only to internal flow is considered, as shown in Fig. 2. The axial force, Q_1, shear force, Q_2, and bending moment, $\mathcal{M}$, on the upper and lower cross-sections are indicated in the same figure. By considering the equilibrium of forces, one obtains

$$\frac{\partial\vec{Q}}{\partial s} + (m+M_i)g\vec{i} = m\frac{\partial^2\vec{r}}{\partial t^2} + M_i\frac{\mathrm{D}^2\vec{r}}{\mathrm{D}t^2}, \tag{11}$$

where Q is the resultant force and $\mathrm{D}(\,)/\mathrm{D}t$ is the material derivative. Similarly, applying a balance of moments leads to

$$\frac{\partial\vec{\mathcal{M}}}{\partial s} + \vec{t}\times\vec{Q} = 0. \tag{12}$$

Since Euler–Bernoulli beam theory is employed, one can make use of the moment–curvature relation given below by neglecting the effect of rotary motion

$$\vec{\mathcal{M}} = EI\vec{t}\times\vec{\bar{\kappa}}. \tag{13}$$

Decomposing $\vec{Q}$ along $\vec{t}$ and $\vec{n}$ gives

$$\vec{Q} = (T_o - A_ip_i)\vec{t} + \vec{t}\times\frac{\partial\vec{\mathcal{M}}}{\partial s}, \tag{14}$$

where T_o is an externally applied tension, p_i is the pressure of the internal fluid, and $A_i = (\pi/4)D_i^2$ is the inner cross-sectional area of the pipe. By substituting Eqs. (13)–(14) into Eqs. (11)–(12) and projecting along x and y, one obtains

$$(m+M_i)g - EI\frac{\partial^4 x}{\partial s^4} + \frac{\partial}{\partial s}\left[(T_o - A_i p_i - EI\bar{\kappa}^2)\frac{\partial x}{\partial s}\right] = m\frac{\partial^2 x}{\partial t^2} + M_i\frac{\mathrm{D}^2 x}{\mathrm{D}t^2}, \quad (15)$$

$$-EI\frac{\partial^4 y}{\partial s^4} + \frac{\partial}{\partial s}\left[(T_o - A_i p_i - EI\bar{\kappa}^2)\frac{\partial y}{\partial s}\right] = m\frac{\partial^2 y}{\partial t^2} + M_i\frac{\mathrm{D}^2 y}{\mathrm{D}t^2}. \quad (16)$$

Integrating Eq. (15) from s to L and dividing it by $\partial x/\partial s$ yields

$$\begin{aligned}(T_o - A_i p_i - EI\bar{\kappa}^2) =& \frac{(m+M_i)g(L-s)}{\partial x/\partial s} + \frac{EI(\partial^3 x/\partial s^3)}{\partial x/\partial s}\\ &+ \frac{[(T_o - A_i p_i)(\partial x/\partial s)]_{s=L}}{\partial x/\partial s}\\ &- \frac{\int_s^L [m(\partial^2 x/\partial t^2) + M_i(\mathrm{D}^2 x/\mathrm{D}t^2)]\,\mathrm{d}s}{\partial x/\partial s}.\end{aligned} \quad (17)$$

Substituting Eq. (17) into Eq. (16) and utilizing the inextensibility condition to eliminate x leads to the same equation of motion obtained via the extended Hamilton's principle, as concluded earlier in [18]. However, the third term on the right-hand side of Eq. (17) was not present in [18], because the pipe was assumed to discharge the fluid to atmosphere and hence there was no tension applied at the free end. By keeping that term and following the same procedure, one obtains the same equation as in [18], but with the following extra term: $-\left[(T_o - A_i p_i)(1 - \frac{1}{2}y'^2)\right]_{s=L}(y'' + \frac{3}{2}y''y'^2)$. This term appears in the final equation of motion obtained in this study.

Moreover, the relation between the external pressure at the free end of the pipe, $p_o(L)$, and the internal one, $p_i(L)$, can be determined by an energy balance of the fluid at $s = L$. Thus,

$$p_i(L) = p_o(L) - \frac{1}{2}\rho U_i^2 + \rho g h_e, \quad (18)$$

where $h_e = K_e U_i^2/(2g)$ is the head-loss due to the sudden enlargement of the flow exiting the pipe into the surrounding fluid, with $K_e = 1$ according to [21].

2.4. Fluid-related forces associated with the external flow in the annular region

In this subsection, the external-fluid part of the problem is analysed in detail. Since the tank, into which the hanging pipe is discharging fluid, is assumed to be large, the external flow velocity over the unconfined region, i.e., before the fluid enters the annular region, is assumed to be $U_o = 0$. However, once the fluid enters the annular region, $U_o \neq 0$; the value of U_o can be determined via continuity as follows: $U_o = U_i(A_i/A_{ch})$, where $A_{ch} = (\pi/4)(D_{ch}^2 - D_o^2)$. In the linear study of [12], the Heaviside step function was utilized to model this discontinuity in the external flow velocity over the length of the pipe; reasonable to good quantitative agreement between the theory and the experiment was achieved in that study. In addition, the logistic function, which provides a smoother transition as compared to the Heaviside step function, was later considered by Abdelbaki et al. [17] to model the discontinuity in the external flow velocity for the same system. An improvement in the capability of the model to predict the threshold of instability and the corresponding frequency of oscillations was reached in [17] as compared to [12]; however, the improvement was only slight. Therefore, since the Heaviside step function results in relatively simpler expressions compared to the logistic one, in the present study it was decided to model the discontinuity in the external flow velocity by means of the Heaviside step function. Hence, one can write $U_o(s) = U_o[1 - \mathrm{H}(s - L')]$.

The fluid-related forces due to the external flowing fluid are derived in a separate manner, as in [22], rather than by the direct application of the Navier–Stokes equations. This approach is well-established in the literature and simplifies the analysis considerably; moreover, it has been shown to give acceptable results, e.g. in [22–26].

The analysis below follows closely the derivation of the model in [26], as the external flow configuration therein is the same as in the problem under study here.

An element of the deformed pipe, at $s \leq L'$, is considered to be subjected only to the external flow; the following set of forces acting on the element, as shown in Fig. 3a, are: the inviscid fluid dynamic force $F_A\delta s$, the normal and longitudinal viscous forces, $F_N\delta s$ and $F_L\delta s$, respectively, and the hydrostatic forces in the x- and y-direction, $F_{px}\delta s$ and $F_{py}\delta s$, respectively.

2.4.1. The inviscid fluid dynamic force, F_A

This force is derived by extending the linear slender-body potential flow theory of Lighthill [27] to a third-order nonlinear formulation. This procedure was elaborated in [19] for a cantilevered cylinder in axial flow, but in the present study the direction of the external flow is reversed; i.e. it is in the opposite direction. Basically, the idea is to assume a velocity potential of the following form: $\phi = -U_o X + \phi_1$, where $-U_o X$ is the potential due to the mean flow, and ϕ_1 is the potential due to the motion of the pipe. First, this potential is determined by satisfying these conditions: (i) the fluid velocity must have a zero value at the outer rigid tube forming the annulus; (ii) the fluid does not penetrate the pipe; and (iii) the solution is 2π-periodic around the pipe, and even with respect to Z. Second, the pressure distribution around the pipe, P, is determined via the Bernoulli equation,

$$P = -\rho\frac{\partial\phi}{\partial t} - \frac{1}{2}\rho(\nabla\phi)^2 + \frac{1}{2}\rho U_o^2, \quad (19)$$

where ρ is the fluid density. As explained in [27], the expression obtained for P in Eq. (19) can be written as $P = P_0 + P_2 + P_1$, where P_0 is the pressure distribution due to the steady flow around an undeformed motionless pipe, P_2 is due to the steady motion of the pipe through a stagnant fluid, and P_1 is the remainder of the pressure distribution. Neither P_0 nor P_2 contributes to a net force on the pipe [19], and in accord with [26], one obtains

$$\begin{aligned}P_1 =& -\rho\left\{\left\{\frac{\partial}{\partial t} + \left[-U_o\left(1 - \frac{\partial u}{\partial X}\right) - \left(\frac{\partial u}{\partial t} - U_o\frac{\partial u}{\partial X}\right)\right]\frac{\partial}{\partial X}\right\}\phi_1\right.\\ &\left. + \frac{1}{2}\left(\frac{\partial\phi_1}{\partial X}\right)^2 - \frac{\partial v}{\partial X}\frac{\partial\phi_1}{\partial Y}\frac{\partial\phi_1}{\partial X}\right\} + \mathcal{O}(\epsilon^5).\end{aligned} \quad (20)$$

Third, the lift force per unit length is determined by $L(X,t) = \oint_{S_X} P_1(-\mathrm{d}Z)$, where S_X is the outer circumference of the pipe. The inviscid force, F_A, has the same magnitude as the lift, but, as used here, it acts in the opposite direction. After straightforward mathematical manipulations, one can obtain

$$\begin{aligned}F_A(X,t) =& \left\{\frac{\partial}{\partial t} + \left[-U_o(1 - \frac{\partial u}{\partial X}) - (\frac{\partial u}{\partial t} - U_o)\frac{\partial u}{\partial X}\right]\frac{\partial}{\partial X}\right\}\\ &\times\left[V_o - (\frac{\partial u}{\partial t}\frac{\partial v}{\partial X} - 2U_o\frac{\partial u}{\partial X}\frac{\partial v}{\partial X}) - \frac{1}{2}V_o(\frac{\partial v}{\partial X})^2\right]M_o\\ &- \frac{1}{2}M_o V_o\frac{\partial v}{\partial X}\frac{\partial V_o}{\partial X} + \mathcal{O}(\epsilon^5),\end{aligned} \quad (21)$$

where V_o is the relative fluid–pipe velocity, $M_o = \chi\rho A_o$ is the virtual added mass, with $\chi = (D_{ch}^2 + D_o^2)/(D_{ch}^2 - D_o^2)$ defined as the confinement parameter [28], and $A_o = \pi D_o^2/4$ is the pipe outer cross-sectional area. In addition, V_o can be defined as $\vec{V}_o = \dot{y}\vec{j} + \dot{x}\vec{i} - (-\vec{U}_f)$, as shown in Fig. 3b, with $U_f = U_o[1 - (\partial u/\partial X)]$ representing the mean axial flow velocity relative to the deforming pipe. The tangential and normal directions to the centreline of the deformed pipe can be represented by the unit vector pair $(\vec{i}_1, \vec{j}_1)$, which is at angle θ_1 to $(\vec{i}, \vec{j})$, as shown in Fig. 3. Thus, θ_1 can be written as

$$\theta_1 = y' - u'y' - \frac{1}{3}y'^3 + \mathcal{O}(\epsilon^5). \quad (22)$$

Projecting V_o on $\vec{j}_1$, the direction normal to the element, leads to $V_o = \dot{y}\cos(\theta_1) + (\dot{x} + U_f)\cos(\bar{\theta}_1)$, where $\bar{\theta}_1 = \frac{1}{2}\pi + \theta_1$. Hence,

$$V_o = \dot{y} - U_o y' - \frac{1}{2}\dot{y}y'^2 + 2U_o u'y' + \frac{1}{2}U_o y'^3 - \dot{x}y' + \mathcal{O}(\epsilon^5). \quad (23)$$

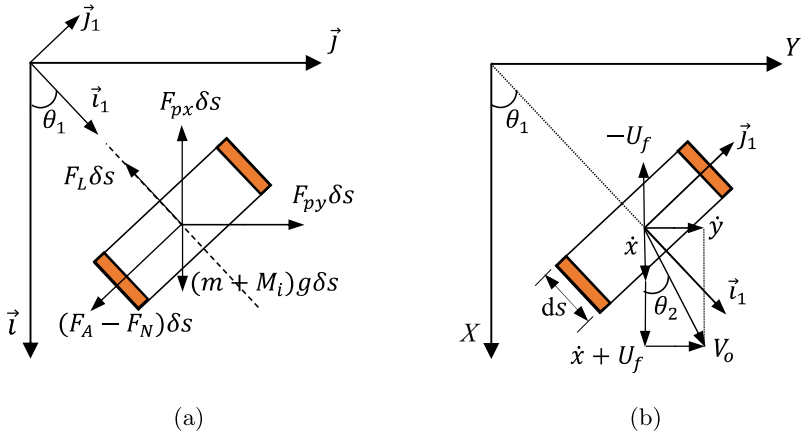

Fig. 3. (a) Fluid-related forces acting on an element of the cantilevered pipe δs; (b) determination of the relative fluid–body velocity V_o associated with the external flow on an element of the pipe.

Finally, to account for the discontinuity in the external flow velocity along s, one can express the inviscid force as follows:

$$\begin{aligned} F_A(X,t) = &\Big\{ \frac{\partial}{\partial t} + \Big[-U_o[1-\mathrm{H}(X-L')](1-\frac{\partial u}{\partial X}) \\ &- (\frac{\partial u}{\partial t} - U_o[1-\mathrm{H}(X-L')])\frac{\partial u}{\partial X} \Big] \frac{\partial}{\partial X} \Big\} \\ &\times \Big[V_o - (\frac{\partial u}{\partial t}\frac{\partial v}{\partial X} - 2U_o[1-\mathrm{H}(X-L')]\frac{\partial u}{\partial X}\frac{\partial v}{\partial X}) \\ &- \frac{1}{2}V_o(\frac{\partial v}{\partial X})^2 \Big] M_o \\ &- \frac{1}{2}M_o V_o \frac{\partial v}{\partial X}\frac{\partial V_o}{\partial X} + \mathcal{O}(\epsilon^5). \end{aligned} \tag{24}$$

Moreover, the expression of the virtual added mass has to be modified to $M_o = [\chi + (1-\chi)\mathrm{H}(s-L')]\rho A_o$, and the linear form of the relative fluid–pipe velocity is expressed as $V_o = \dot{y} - U_o[1-\mathrm{H}(s-L')]y'$.

2.4.2. The viscous forces F_N and F_L

These forces are derived on the basis of the semi-empirical formulas provided by Taylor [29], which are suitable for the degree of confinement of the flow considered in this problem; i.e., not too severe, as discussed in [19]. The expressions given in [29] are

$$F_N = \frac{1}{2}\rho D_o U_o^2 (C_N \sin i + C_{Dp}\sin^2 i), \quad F_L = \frac{1}{2}\rho D_o U_o^2 C_T \cos i, \tag{25}$$

where C_N and C_T are friction coefficients in the normal and tangential directions of the pipe centreline, respectively; C_{Dp} is a form-drag coefficient and the term $\frac{1}{2}\rho D_o U_o^2 C_{Dp}\sin^2 i$ is the normal steady hydrodynamic force per unit length, also known as a vortex-lift term — see [30]; i is the angle of attack, which can be determined by $i = \theta_1 - \theta_2$, as indicated in Fig. 3b, with $\theta_2 = \tan^{-1}\{(\partial y/\partial t)/[U_f + (\partial x/\partial t)]\}$. By following the framework presented in [19,26] and taking into account the difference in the value of $U_o(s)$ outside and inside the annular region, the normal and longitudinal viscous forces can be expressed as

$$\begin{aligned} F_N = &\frac{1}{2}\rho D_o U_o^2[1-\mathrm{H}(s-L')]\Big[C_N\Big(y' - \frac{\dot{y}}{U_o} - \frac{\dot{y}u'}{U_o} - u'y' + \frac{\dot{x}\dot{y}}{U_o^2} \\ &- \frac{1}{2}\Big(y'^3 - \frac{\dot{y}^3}{U_o^3} - \frac{y'^2\dot{y}}{U_o} + \frac{y'\dot{y}^2}{U_o^2}\Big)\Big) \\ &- C_{Dp}\Big(y'|y'| + \frac{y'|\dot{y}| + |y'|\dot{y}}{U_o} + \frac{\dot{y}|\dot{y}|}{U_o^2}\Big)\Big] - k\dot{y} + \mathcal{O}(\epsilon^5), \\ F_L = &\frac{1}{2}\rho D_o U_o^2[1-\mathrm{H}(s-L')]C_T\Big[1 - \frac{1}{2}\Big(y'^2 - 2\frac{y'\dot{y}}{U_o} + \frac{\dot{y}^2}{U_o^2}\Big)\Big] + \mathcal{O}(\epsilon^4). \end{aligned} \tag{26}$$

It should be noted that the quadratic terms associated with the form-drag coefficient were modified in a similar way as in [19,31] to obtain forces that are always opposing motion. Also a viscous damping term, $k\dot{y}$, has been added, based on the analysis in [12,24]. The value of the viscous damping coefficient, k, should be dependent on the frequency of oscillations and the degree of confinement of the surrounding flow [12,32,33]. One can make use of the following expression provided in [12]: $k = k_u(1+\bar{\gamma}^3)/(1-\bar{\gamma}^2)^2$, in which $\bar{\gamma} = D_o/D_{ch}$ and $k_u = 2\sqrt{2}\rho A_o \mathcal{R}(\Omega)/\sqrt{S}$, where $\mathcal{R}(\Omega)$ is the circular frequency of oscillations, $S = \mathcal{R}(\Omega)D_o^2/4\nu$ is the Stokes number, also known as the oscillatory Reynolds number, and ν is the kinematic viscosity of the fluid. Here, this expression of viscous damping coefficient is modified to account for the difference between the confined and unconfined regions of the flow around the pipe, and thus

$$k = k_u\Big[\frac{1+\bar{\gamma}^3}{(1-\bar{\gamma}^2)^2} + \mathrm{H}(s-L')\Big(1 - \frac{1+\bar{\gamma}^3}{(1-\bar{\gamma}^2)^2}\Big)\Big]. \tag{27}$$

2.4.3. The hydrostatic forces F_{px} and F_{py}

These forces are the resultants of the external steady-state pressure p_o acting on the pipe. The procedure described in [19,24] for a cantilevered cylinder in axial flow is used to derive nonlinear expressions for these forces, taking into account the inverse direction of the annular flow in the problem under study. The idea is to assume a momentarily frozen element, δs, of the pipe immersed in the fluid with F_{px} and F_{py} acting on the two normally wet surfaces, as well as $p_o A_o$ and $p_o A_o + [\partial(p_o A_o)/\partial s]\delta s$ acting on the normally dry surfaces. The net resultant of all these forces is known: it is the buoyancy force. By subtracting the known forces from the buoyancy resultant, one obtains the forces desired here. The pressure gradient in the outer flow for the problem in hand can be expressed as follows:

$$\begin{aligned} A_o\Big(\frac{\partial p_o}{\partial x}\Big) = &\frac{1}{2}\rho D_o U_o^2[1-\mathrm{H}(X-L')]C_T\frac{D_o}{D_h} + \rho g A_o + A_o\Big(\frac{1}{2}\rho U_o^2 + \rho g h_a\Big) \\ &\times \delta_D(X-L'), \end{aligned} \tag{28}$$

where $D_h = D_{ch} - D_o$ is the hydraulic diameter, δ_D is the Dirac delta function, and $h_a = K_1 U_o^2/(2g)$ is the head-loss associated with the stagnant fluid entering the annular region, with $0.8 \le K_1 \le 0.9$ [21]. By rewriting the derivative in Eq. (28) with respect to X and integrating from $X = s$ to L, one can obtain:

$$\begin{aligned} A_o p_o(s) = &A_o p_o(L) - \Big(\frac{1}{2}\rho D_o U_o^2[1-\mathrm{H}(s-L')]C_T\frac{D_o}{D_h}\Big) \\ &\times\Big[(L'-s) - \int_s^L \frac{1}{2}y'^2 \mathrm{d}s\Big] \\ &- \rho g A_o\Big[(L-s) - \int_s^L \frac{1}{2}y'^2\mathrm{d}s\Big] - A_o\Big(\frac{1}{2}\rho U_o^2 + \rho g h_a\Big) \\ &\times[1-\mathrm{H}(s-L')] \\ &+ A_o\Big(\frac{1}{2}\rho U_o^2 + \rho g h_a\Big)\int_s^L \frac{1}{2}y'^2\delta_D(s-L')\mathrm{d}s + \mathcal{O}(\epsilon^4). \end{aligned} \tag{29}$$

Proceeding with the derivation, following the procedure utilized in [19], and by using Eqs. (28) and (29), the following expressions for the hydrostatic forces are obtained:

$$\begin{aligned}
-F_{px} &= y'^2\left(-\frac{1}{2}\rho D_o U_o^2[1-\mathrm{H}(s-L')]C_T\frac{D_o}{D_h}-\rho g A_o\right.\\
&\quad\left.-A_o\left(\frac{1}{2}\rho U_o^2+\rho g h_a\right)\delta_D(s-L')\right)-y'y''A_o p_o+\mathcal{O}(\epsilon^4),\\
F_{py} &= (y'-u'y'-y'^3)\left(\frac{1}{2}\rho D_o U_o^2[1-\mathrm{H}(s-L')]C_T\frac{D_o}{D_h}\right.\\
&\quad+\rho g A_o+A_o\left(\frac{1}{2}\rho U_o^2+\rho g h_a\right)\delta_D(s-L')\Big)\\
&\quad+(y''-u''y'-u'y''-\frac{3}{2}y'^2y'')A_o p_o+\mathcal{O}(\epsilon^5).
\end{aligned}\tag{30}$$

2.5. Virtual work due to the fluid-related forces associated with the external flow

Referring to Fig. 3a, an expression for the virtual work done on the pipe by the external-fluid-related forces can be written as

$$\begin{aligned}
\int_{t_1}^{t_2}\delta W_o\mathrm{d}t = \int_{t_1}^{t_2}\int_0^L\{&[-F_{px}-F_L\cos\theta_1+(F_A-F_N)\sin\theta_1]\delta x\\
&+[F_{py}-F_L\sin\theta_1-(F_A-F_N)\cos\theta_1]\delta y\}\,\mathrm{d}s\,\mathrm{d}t.
\end{aligned}\tag{31}$$

By substituting Eqs. (24), (26) and (30) into Eq. (31), and with the aid of Eqs. (7) and (22), the virtual work can finally be determined — not given here for brevity.

2.6. Equation of motion and boundary conditions

The following nonlinear equation of motion for the pipe can be obtained by substituting Eqs. (4), (6), (10), and the final form of Eq. (31) into Eq. (2), after many straightforward but tedious manipulations and transformations, and by truncating to third order of magnitude:

$$\begin{aligned}
&\{m+M_i+[\chi+(1-\chi)\mathrm{H}(s-L')]\rho A_o\}\ddot{y}+2M_iU_i\dot{y}'(1+y'^2)\\
&-2\chi\rho U_o[1-\mathrm{H}(s-L')]\dot{y}'\left(1-\frac{1}{4}y'^2\right)\\
&+M_iU_i^2y''(1+y'^2)+\chi\rho U_o^2[1-\mathrm{H}(s-L')]y''(1+2y'^2)\\
&-\frac{3}{2}[\chi+(1-\chi)\mathrm{H}(s-L')]\rho A_o\dot{y}y'\dot{y}'\\
&+\frac{3}{2}[\chi+(1-\chi)\mathrm{H}(s-L')]\rho A_oU_o[1-\mathrm{H}(s-L')]\dot{y}y'y''\\
&-\frac{1}{2}\rho D_oU_o^2[1-\mathrm{H}(s-L')]C_N\left(y'+\frac{1}{2}y'^3\right)\\
&+\frac{1}{2}\rho D_oU_o^2[1-\mathrm{H}(s-L')]C_T(L'-s)\left(y''+\frac{3}{2}y'^2y''\right)\\
&-Ap_o(L)(y''+y'^2y'')\\
&-\left[(T_o-A_ip_i)(1-\frac{1}{2}y'^2)\right]_{s=L}(y''+\frac{3}{2}y'^2y'')\\
&-\left\{\frac{1}{2}\rho D_oU_o^2[1-\mathrm{H}(s-L')]C_T\frac{D_o}{D_h}-(m+M_i)g+\rho gA_o\right.\\
&\left.+A_o\left(\frac{1}{2}\rho U_o^2+\rho gh_a\right)\delta_D(s-L')\right\}\left(y'+\frac{1}{2}y'^3\right)\\
&+\frac{1}{2}\rho D_oU_o^2[1-\mathrm{H}(s-L')]C_T\frac{D_o}{D_h}(L'-s)\\
&\times\left(y''+\frac{3}{2}y'^2y''\right)+[\rho gA_o-(m+M_i)g](L-s)\left(y''+\frac{3}{2}y'^2y''\right)\\
&+A_o\left(\frac{1}{2}\rho U_o^2+\rho gh_a\right)[1-\mathrm{H}(s-L')]\\
&\times\left(y''+\frac{1}{2}y'^2y''\right)+EI(y''''+4y'y''y'''+y''^3+y''''y'^2)\\
&+\frac{1}{2}\rho D_oC_N\dot{y}\int_0^s y'\dot{y}'\,\mathrm{d}s\\
&+\frac{1}{2}\rho D_oU_o^2[1-\mathrm{H}(s-L')]C_N\left(\frac{\dot{y}}{U_o}+\frac{1}{2}\frac{y'\dot{y}^2}{U_o^2}-\frac{1}{2}\frac{y'^2\dot{y}}{U_o}-\frac{\dot{y}^3}{2U_o^3}\right)\\
&+\frac{1}{2}\rho D_oU_o^2[1-\mathrm{H}(s-L')]C_{Dp}\left(y'|y'|+\frac{y'|\dot{y}|+|y'|\dot{y}}{U_o}+\frac{\dot{y}|\dot{y}|}{U_o^2}\right)\\
&+k\dot{y}-(m+M_i)y''\int_s^L\int_0^s(\dot{y}'^2+y'\ddot{y}')\,\mathrm{d}s\,\mathrm{d}s\\
&+2[\chi+(1-\chi)\mathrm{H}(s-L')]\rho A_o\dot{y}'\int_0^s y'\dot{y}'\,\mathrm{d}s\\
&-2\chi\rho A_oU_o[1-\mathrm{H}(s-L')]y''\dot{y}'\int_0^s y'\dot{y}'\,\mathrm{d}s\\
&-[\chi+(1-\chi)\mathrm{H}(s-L')]\rho A_oy''\int_s^L\{\ddot{y}y'\\
&-2U_o[1-\mathrm{H}(s-L')]y'\dot{y}'+U_o^2y'y''[1-\mathrm{H}(s-L')]\}\,\mathrm{d}s\\
&+\{m+M_i+[\chi+(1-\chi)\mathrm{H}(s-L')]\rho A_o\}y'\int_0^s(y'\ddot{y}'+\dot{y}'^2)\,\mathrm{d}s\\
&-3\chi\rho A_oU_o[1-\mathrm{H}(s-L')]y'\int_0^s(y'\dot{y}''+y''\dot{y}')\,\mathrm{d}s\\
&+y''\int_s^L\{Ap_o(L)y'y''-\frac{1}{4}\rho D_oC_T\dot{y}^2\}\,\mathrm{d}s\\
&-\frac{1}{2}\rho D_oU_o^2y''(C_T-C_N)\int_s^L\left(y'^2-\frac{y'\dot{y}}{U_o}\right)[1-\mathrm{H}(s-L')]\,\mathrm{d}s\\
&-y''\int_s^L(2M_iU_iy'\dot{y}'+M_iU_i^2y'y'')\,\mathrm{d}s\\
&-\frac{1}{4}y''\rho D_oU_o^2C_T\frac{D}{D_h}\int_s^L y'^2[(L'-s)\delta_D(s-L')-\mathrm{H}(s-L')]\,\mathrm{d}s\\
&-y''A_o\left(\frac{1}{2}\rho U_o^2+\rho gh_a\right)\int_s^L y'y''\,\mathrm{d}s=0.
\end{aligned}\tag{32}$$

The boundary conditions are the classical ones for a cantilevered beam, namely

$$y(0)=0,\ y'(0)=0,\ y''(L)=0,\text{and }y'''(L)=0.\tag{33}$$

Defining next the dimensionless quantities

$$\begin{aligned}
&\xi=\frac{s}{L},\quad \eta=\frac{y}{L},\quad \tau=\left(\frac{EI}{m+M_i+\rho A_o}\right)^{1/2}\frac{t}{L^2},\quad u_i=\left(\frac{M_i}{EI}\right)^{1/2}U_iL,\\
&u_o=\left(\frac{\rho A_o}{EI}\right)^{1/2}U_oL,\quad \beta_i=\frac{M_i}{m+M_i+\rho A_o},\quad \beta_o=\frac{\rho A_o}{m+M_i+\rho A_o},\\
&\gamma=\frac{(m+M_i-\rho A_o)gL^3}{EI},\quad \Gamma=\frac{T_o(L)L^2}{EI},\quad c_N=\frac{4}{\pi}C_N,\quad c_T=\frac{4}{\pi}C_T,\\
&c_d=\frac{4}{\pi}C_{Dp},\quad \varepsilon=\frac{L}{D_o},\quad h=\frac{D_o}{D_h},\quad \alpha=\frac{D_i}{D_o},\quad \alpha_{ch}=\frac{D_{ch}}{D_o},\quad r_{ann}=\frac{L'}{L},\\
&\Pi_{iL}=\frac{A_ip_i(L)L^2}{EI},\quad \Pi_{oL}=\frac{A_op_o(L)L^2}{EI},\quad \kappa=\frac{kL^2}{[EI(m+M_i+\rho A_o)]^{1/2}},
\end{aligned}\tag{34}$$

the equation of motion can be written in the following dimensionless form:

$$\begin{aligned}
&\{1+\beta_o(\chi-1)[1-\mathrm{H}(\xi-r_{ann})]\}\ddot{\eta}+2u_i\sqrt{\beta_i}\dot{\eta}'(1+\eta'^2)\\
&-2\chi u_o\sqrt{\beta_o}[1-\mathrm{H}(\xi-r_{ann})]\dot{\eta}'(1-\frac{1}{4}\eta'^2)\\
&+u_i^2\eta''(1+\eta'^2)+\chi u_o^2[1-\mathrm{H}(\xi-r_{ann})]\eta''(1+2\eta'^2)\\
&-\frac{3}{2}[\chi+(1-\chi)\mathrm{H}(\xi-r_{ann})]\beta_o\dot{\eta}\eta'\dot{\eta}'\\
&+\frac{3}{2}\chi u_o[1-\mathrm{H}(\xi-r_{ann})]\sqrt{\beta_o}\dot{\eta}\eta'\eta''-\frac{1}{2}u_o^2[1-\mathrm{H}(\xi-r_{ann})]\varepsilon c_N[\eta'+\frac{1}{2}\eta'^3]
\end{aligned}$$

$$
\begin{aligned}
&+\frac{1}{2}u_o^2[1-\mathrm{H}(\xi-r_{ann})]\varepsilon c_T(r_{ann}-\xi)(\eta''+\frac{3}{2}\eta'^2\eta'')-\Pi_{oL}(\eta''+\eta'^2\eta'')\\
&-(\Gamma-\Pi_{iL})(\eta''+\frac{3}{2}\eta'^2\eta'')\\
&+\frac{1}{2}(\Gamma-\Pi_{iL})\eta''\left[\eta'^2\right]_{\xi=1}-\Big\{\frac{1}{2}u_o^2[1-\mathrm{H}(\xi-r_{ann})]\varepsilon c_T h-\gamma\\
&+\frac{1}{2}u_o^2(1+K_1)\delta_D(\xi-r_{ann})\Big\}(\eta'+\frac{1}{2}\eta'^3)\\
&+\frac{1}{2}u_o^2[1-\mathrm{H}(\xi-r_{ann})]\varepsilon c_T h(r_{ann}-\xi)(\eta''+\frac{3}{2}\eta'^2\eta'')\\
&-\gamma(1-\xi)(\eta''+\frac{3}{2}\eta'^2\eta'')\\
&+\frac{1}{2}u_o^2(1+K_1)[1-\mathrm{H}(\xi-r_{ann})](\eta''+\frac{1}{2}\eta'^2\eta'')\\
&+\eta''''+4\eta'\eta''\eta'''+\eta''^3+\eta''''\eta'^2\\
&+\frac{1}{2}\varepsilon c_N\beta_o\dot\eta\int_0^\xi\eta'\dot\eta'\,\mathrm{d}s+\frac{1}{2}u_o^2[1-\mathrm{H}(\xi-r_{ann})]\varepsilon c_N\Big(\frac{\sqrt{\beta_o}}{u_o}\dot\eta+\frac{1}{2}\frac{\beta_o}{u_o^2}\dot\eta^2\eta'\\
&-\frac{1}{2}\frac{\sqrt{\beta_o}}{u_o}\dot\eta\eta'^2-\frac{1}{2}\frac{\beta_o^{3/2}}{u_o^3}\dot\eta^3\Big)\\
&+\frac{1}{2}u_o^2[1-\mathrm{H}(\xi-r_{ann})]\varepsilon c_d\Big(\eta'|\eta'|+\frac{\sqrt{\beta_o}}{u_o}(\eta'|\dot\eta|+|\eta'|\dot\eta)+\frac{\beta_o}{u_o}\dot\eta|\dot\eta|\Big)+\kappa\dot\eta\\
&-\eta''(1-\beta_o)\int_\xi^1\int_0^\xi(\dot\eta'^2+\eta'\ddot\eta')\,\mathrm{d}\xi\,\mathrm{d}\xi\\
&+2[\chi+(1-\chi)\mathrm{H}(\xi-r_{ann})]\beta_o\dot\eta'\int_0^\xi\eta'\dot\eta'\,\mathrm{d}\xi\\
&-2\chi\sqrt{\beta_o}u_o[1-\mathrm{H}(\xi-r_{ann})]\eta''\int_0^\xi\eta'\dot\eta'\,\mathrm{d}\xi\\
&-[\chi+(1-\chi)\mathrm{H}(\xi-r_{ann})]\eta''\int_\xi^1\Big\{\beta_o\ddot\eta\eta'\\
&-2u_o\sqrt{\beta_o}[1-\mathrm{H}(\xi-r_{ann})]\dot\eta'\eta'+u_o^2[1-\mathrm{H}(\xi-r_{ann})]\eta''\eta'\Big\}\,\mathrm{d}\xi\\
&+\{1+(\chi-1)\beta_o[1-\mathrm{H}(\xi-r_{ann})]\}\eta'\int_0^\xi(\dot\eta'^2+\eta'\ddot\eta')\,\mathrm{d}\xi\\
&-3\chi\sqrt{\beta_o}u_o[1-\mathrm{H}(\xi-r_{ann})]\eta'\int_0^\xi(\eta'\dot\eta''+\eta''\dot\eta')\,\mathrm{d}\xi\\
&+\eta''\int_\xi^1\{\Pi_{oL}\eta'\eta''-\frac{1}{4}\varepsilon c_T\beta_o\dot\eta^2\}\,\mathrm{d}\xi\\
&-\frac{1}{2}u_o^2(\varepsilon c_T-\varepsilon c_N)\eta''\int_\xi^1(\eta'^2-\frac{\sqrt{\beta_o}}{u_o}\eta'\dot\eta)[1-\mathrm{H}(\xi-r_{ann})]\,\mathrm{d}\xi\\
&-\eta''\int_\xi^1(2u_i\sqrt{\beta_i}\eta'\dot\eta'+u_i^2\eta'\eta'')\,\mathrm{d}\xi\\
&-\frac{1}{4}u_o^2\varepsilon c_T h\eta''\int_\xi^1\eta'^2[(r_{ann}-\xi)\delta_D(\xi-r_{ann})-\mathrm{H}(\xi-r_{ann})]\,\mathrm{d}\xi\\
&-\frac{1}{2}u_o^2(1+K_1)\eta''\int_\xi^1\eta'\eta''\mathrm{d}\xi=0,
\end{aligned}
\tag{35}
$$

where $(\,)'=\partial(\,)/\partial\xi$ and $\dot{(\,)}=\partial(\,)/\partial\tau$. The viscous damping coefficient may be expressed in dimensionless form as follows: $\kappa=\kappa_u\big\{1+[1-\mathrm{H}(\xi-r_{ann})][(1+\alpha_{ch}^{-3})/(1-\alpha_{ch}^{-2})^2-1]\big\}$.

2.7. Methods of analysis

The Galerkin technique is employed to discretize the partial differential equation of motion (35) into a set of ordinary differential equations (ODEs). Thus, $\eta(\xi,\tau)=\sum_{j=1}^{N}\phi_j(\xi)q_j(\tau)$. In the Galerkin scheme, N represents the number of comparison functions used in the analysis; $\phi_j(\xi)$, with $j=1:N$, are the comparison functions, which are chosen to be the cantilever-beam eigenfunctions, as they satisfy the boundary conditions; $q_j(\tau)$ are the corresponding generalized coordinates. The resultant equations are then multiplied by $\phi_i(\xi)$, with $i=1:N$, and integrated over the domain $[0:1]$, which leads to the following ODEs:

$$
\begin{aligned}
&M_{ij}\ddot q_j+C_{ij}\dot q_j+K_{ij}q_j+r_{ijk}q_j|q_k|+\bar s_{ijk}|q_j|\dot q_k+\tilde s_{ijk}q_j|\dot q_k|+t_{ijk}\dot q_j|\dot q_k|\\
&+\alpha_{ijkl}q_jq_kq_l+\beta_{ijkl}q_jq_k\dot q_l+\gamma_{ijkl}q_j\dot q_k\dot q_l+\eta_{ijkl}\dot q_j\dot q_k\dot q_l+\mu_{ijkl}q_jq_k\ddot q_l=0,
\end{aligned}
\tag{36}
$$

in which the repetition of an index implies summation. The coefficients of the linear terms: M_{ij}, C_{ij} and K_{ij} correspond to the mass, damping and stiffness matrices, respectively; they are given by

$$
\begin{aligned}
M_{ij}&=a_{ij_{(0,1)}}-\beta_o(1-\chi)a_{ij_{(0,r_{ann})}},\\
C_{ij}&=2u_i\sqrt{\beta_i}b_{ij_{(0,1)}}-2\chi u_o\sqrt{\beta_o}b_{ij_{(0,r_{ann})}}+\frac{1}{2}u_o\varepsilon c_N\sqrt{\beta_o}a_{ij_{(0,r_{ann})}}\\
&\quad+\kappa_u a_{ij_{(0,1)}}+\kappa_u\left[\frac{1+\alpha_{ch}^{-3}}{(1-\alpha_{ch}^{-2})^2}-1\right]a_{ij_{(0,r_{ann})}},\\
K_{ij}&=\lambda_j^4a_{ij_{(0,1)}}+\gamma b_{ij_{(0,1)}}-\frac{1}{2}u_o^2\varepsilon c_T h b_{ij_{(0,r_{ann})}}-\frac{1}{2}u_o^2\varepsilon c_N b_{ij_{(0,r_{ann})}}\\
&\quad-\frac{1}{2}u_o^2(1+K_1)(\phi_i|_{\xi=r_{ann}}\phi_j'|_{\xi=r_{ann}})\\
&\quad-(\Gamma-\Pi_{iL}+\Pi_{oL})c_{ij_{(0,1)}}-\gamma(c_{ij_{(0,1)}}-d_{ij_{(0,1)}})\\
&\quad+\frac{1}{2}u_o^2\varepsilon c_T(1+h)(r_{ann}c_{ij_{(0,1)}}-d_{ij_{(0,1)}})+\frac{1}{2}u_o^2(1+K_1^2)c_{ij_{(0,r_{ann})}}\\
&\quad+u_i^2c_{ij_{(0,1)}}+\chi u_o^2c_{ij_{(0,r_{ann})}},
\end{aligned}
\tag{37}
$$

where λ_j is the jth eigenvalue of the dimensionless cantilevered beam characteristic equation, and the constants a_{ij}, b_{ij}, c_{ij} and d_{ij} are defined as follows [34]:

$$
\begin{aligned}
a_{ij_{(a,b)}}&=\int_a^b\phi_i\phi_j\,\mathrm{d}\xi,\quad b_{ij_{(a,b)}}=\int_a^b\phi_i\phi_j'\,\mathrm{d}\xi,\\
c_{ij_{(a,b)}}&=\int_a^b\phi_i\phi_j''\,\mathrm{d}\xi,\quad d_{ij_{(a,b)}}=\int_a^b\xi\phi_i\phi_j''\,\mathrm{d}\xi.
\end{aligned}
\tag{38}
$$

For convenience, the rather long expressions of the nonlinear coefficients, r_{ijk}, $\bar s_{ijk}$, $\tilde s_{ijk}$, t_{ijk}, α_{ijkl}, β_{ijkl}, γ_{ijkl}, η_{ijkl} and μ_{ijkl} are given in Appendix.

3. Results of the theoretical model

In this section, the discretized ODEs obtained in Section 2 are solved for two different flexible pipes, the dimensions and material characteristics of which are listed in Table 1. Also, the internal diameter of the rigid tube forming the annulus surrounding the pipes is taken to be $D_{ch}=31.5$ mm; its length can have one of the following three values: 109 mm, 206.5 mm, 304.5 mm. The corresponding dimensionless parameters of the two systems under study are listed in Table 2. In addition, the confinement length parameter, $r_{ann}=L'/L$, corresponding to the different lengths of the annular region, is $r_{ann}=0.253$, 0.478, 0.705 for Pipe 1, and $r_{ann}=0.246$, 0.467, 0.688 for Pipe 2. The value of the form-drag coefficient due to the external flow inside the annular region is taken as $C_{Dp}=1.1$, as in [29]. Also, the normal and tangential friction coefficients are assumed to be $C_N=C_T=0.0125$, as in [5,12]. In addition, the viscous damping coefficient, κ_u, is given a constant value for each mode j. This value is determined based on the average frequency of oscillations for each mode[2] over a specific range of interest of the internal flow velocity, u_i. Thus, the values of κ_u for six modes, i.e. $N=6$, are $\kappa_{uj}=\{0.36, 0.81, 1.43, 2.02, 2.60, 3.18\}$ for Pipe 1 and $\kappa_{uj}=\{0.43, 0.99, 1.83, 2.61, 3.39, 4.16\}$ for Pipe 2.[3] The ODEs are solved by employing the pseudo-arclength continuation

[2] The frequency of oscillation for each mode is obtained via a linear analysis of the problem at hand, solving the eigenvalue problem, and taking an average value, over a specific range of flow velocities, of the real part of the dimensionless eigenfrequency for each mode, $\mathcal{R}(\omega_i)$, where $i=1:N$.

[3] These values for κ_u were calculated for an annular region of 109 mm length; they were recalculated for the other lengths of the annulus.

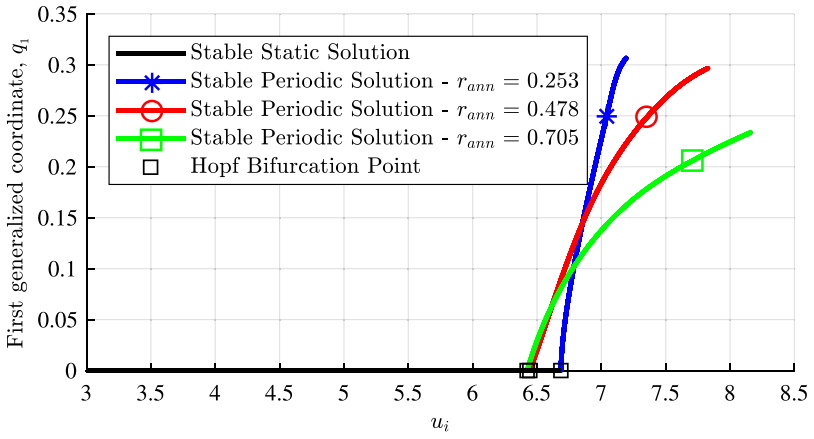

Fig. 4. Bifurcation diagrams for Pipe 1 with different lengths of the annular region showing the first generalized coordinate, q_1, as a function of the dimensionless internal flow velocity, u_i.

Table 1
Properties of the flexible pipes.

Pipe	Material	D_i (mm)	D_o (mm)	L (mm)	EI (N m^2)	m (kg m^{-1})
1	Silicone-rubber	6.35	16	431	7.37×10^{-3}	0.194
2	Thermoplastic-rubber	6.35	9.53	443	9.33×10^{-3}	4.07×10^{-2}

Table 2
Dimensionless parameters of the two systems under study.

System	α	α_{ch}	β_i	β_o	γ	ϵ	h
Pipe 1	0.397	1.97	7.41×10^{-2}	0.470	2.69	26.9	1.03
Pipe 2	0.666	3.31	0.22	0.496	0.104	46.5	0.434

method using AUTO [35], which is adapted to conduct bifurcation analysis for differential equations, and also via the MATLAB ODE solver (Mathworks, Inc.) for direct time-integration purposes.

3.1. Results for Pipe 1

Fig. 4 shows bifurcation diagrams obtained via AUTO using a six-mode Galerkin approximation[4]; the first generalized coordinate, q_1, which is considered to be representative of the behaviour of the system, is plotted versus the dimensionless internal flow velocity, u_i. The figure shows the dynamical behaviour of Pipe 1 for different lengths of the annular region. For $r_{ann} = 0.253$, the pipe remains stable around the original equilibrium state for all $u_i < 6.69$. At $u_i \approx 6.69$, a Hopf bifurcation is predicted that leads to stable periodic oscillations around the origin, corresponding to flutter in the second mode of the pipe. The maximum value of q_1 is plotted in Fig. 4, and it increases with increasing flow velocity u_i. At $u_i > 7.19$, the model fails to converge to any stable solution, perhaps because the large amplitude of oscillation involved requires a finer model than one correct only to third-order accuracy. However, at a value of u_i less than that, $u_i \approx 6.77$, the pipe is predicted to start hitting the annulus-forming tube, as shown in Fig. 5a, and this eventuality is not accounted for in the model. Increasing the length of the annular region destabilizes the system; i.e., it causes the flutter to occur at lower flow velocities, as shown in Fig. 4, and decreases the amplitude of oscillation at higher flow velocities, beyond the onset of flutter. It is clear from Fig. 5 that the flutter predicted for this system is in the second mode of the pipe.

The nonlinear dynamics of the pipe with different lengths of the annular region are examined right before the pipe starts hitting the outer rigid tube. Samples of time histories obtained using the MATLAB ODE solver are shown in Figs. 6–8 for $r_{ann} = 0.253$, $r_{ann} = 0.478$ and $r_{ann} = 0.705$, respectively; these time histories are calculated at a point very close to the free end of the pipe; i.e. at $\xi = 0.97$. In addition, phase-plane, and power-spectral-density (PSD) plots calculated by direct fast Fourier transform (FFT) are shown in the same figures. All of these plots indicate regular periodic motions with one dominant frequency of oscillation; the other strong peaks that appear in the PSD plots, in Figs. 6c and 7c, correspond to the third and fifth harmonics of the main frequency.

The frequency of oscillation, f, is plotted against the dimensional internal flow velocity U_i in Fig. 9; it is seen that increasing the length of the annular region decreases the frequency of oscillation, as a result of the increase in the added mass. On the other hand, increasing the flow velocity increases the frequency of oscillation slightly.

3.2. Results for Pipe 2

The dynamical behaviour for Pipe 2 with increasing flow velocity is similar to that obtained for Pipe 1. In general, the pipe loses stability via flutter in the second mode with increasing internal flow velocity u_i. Bifurcation diagrams for the pipe with different values of r_{ann} are shown in Fig. 10. As concluded for Pipe 1, increasing the level of confinement by increasing the length of the annular region destabilizes the system and significantly decreases the amplitude of oscillation at high flow velocities. Furthermore, from Fig. 10, one can see that the amplitude of oscillation increases with increasing flow velocity, and the pipe starts to hit the external tube at high enough flow velocities, as shown in Fig. 11. The nonlinear dynamic characteristics of the system at these flow velocities are illustrated in Figs. 12–14 for a point located at $\xi = 0.98$; again, simple periodic motions are predicted with one dominant frequency of oscillation. This frequency is plotted versus U_i in Fig. 15. Interestingly, for this pipe, the level of confinement and the flow velocity do not significantly affect the frequency of oscillation; increasing the former, slightly decreases the frequency, while increasing the latter slightly increases it, for flow velocities higher than the onset of instability.

4. Comparison between the results of the present model and other studies from the literature

4.1. Critical flow velocities, frequencies and amplitudes of flutter

The two sets of parameters used to solve the equation of motion were purposely chosen to allow comparison between the results obtained by this nonlinear model and experimental observations, as well as the theoretical predictions by Moditis et al. [12] for the bench-top-size system. It was observed experimentally and determined by a linear

[4] The number of modes was increased till convergence was achieved; the convergence criterion for the onset of instability and the amplitude of oscillations was set at 5%.

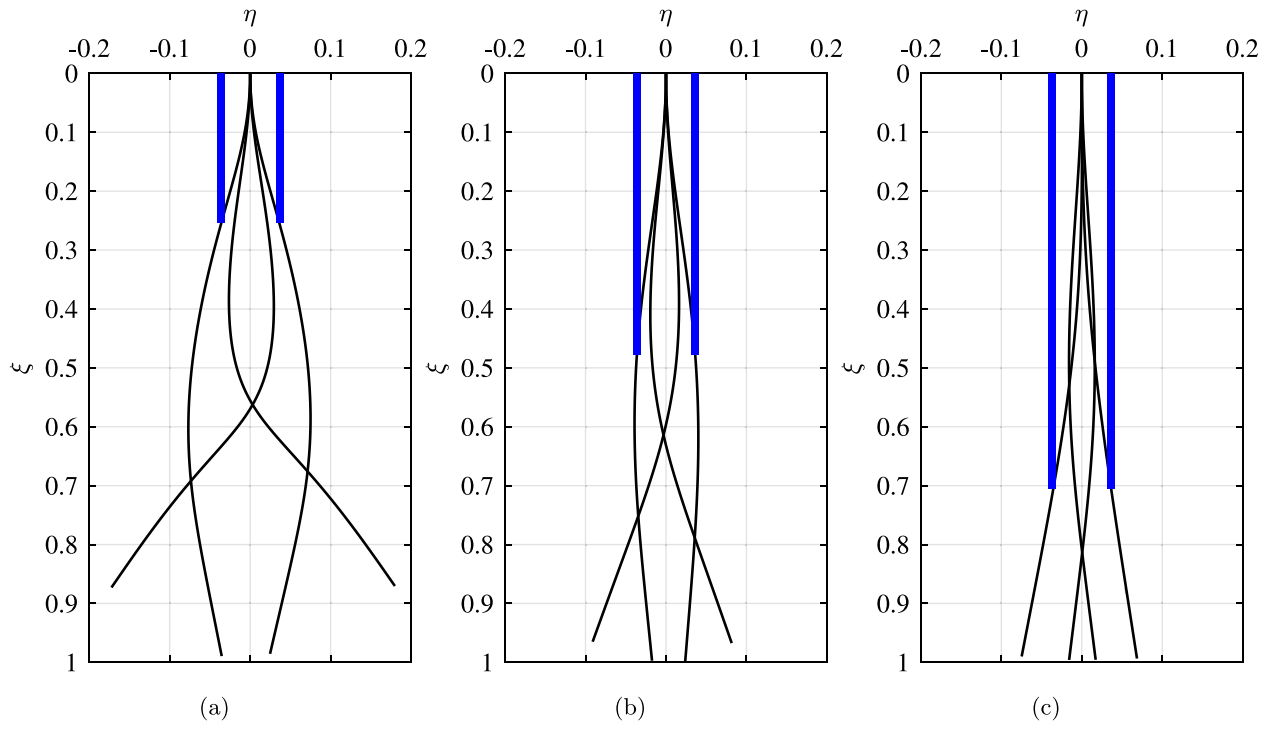

Fig. 5. Shapes of the oscillating Pipe 1 just before impacting the annulus-forming tube for: (a) $r_{ann} = 0.253$ at $u_i = 6.77$, (b) $r_{ann} = 0.478$ at $u_i = 6.57$, and (c) $r_{ann} = 0.705$ at $u_i = 6.51$.

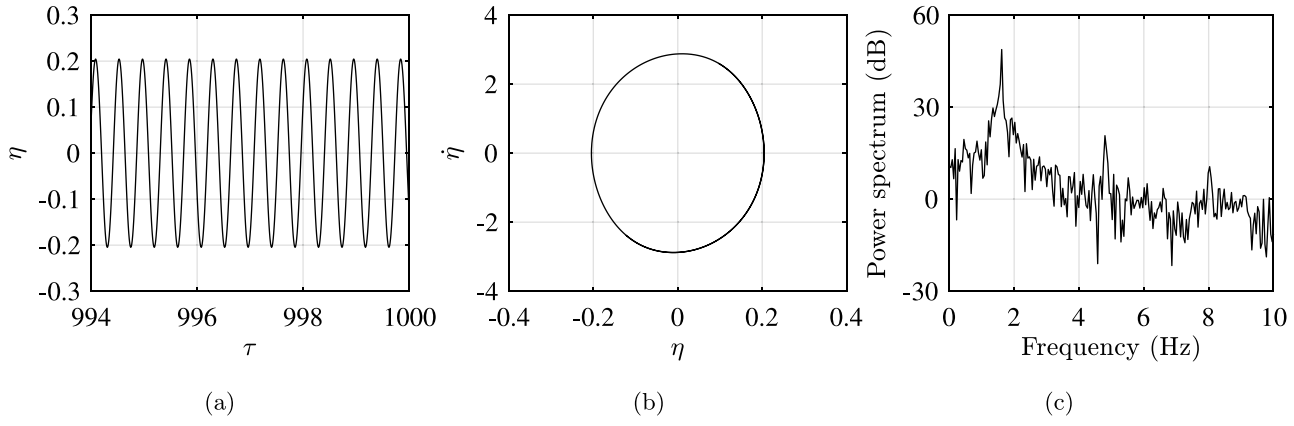

Fig. 6. (a) Time history plot, (b) phase-plane plot, and (c) power spectral density plot of Pipe 1 at $u_i = 6.77$ for $r_{ann} = 0.253$.

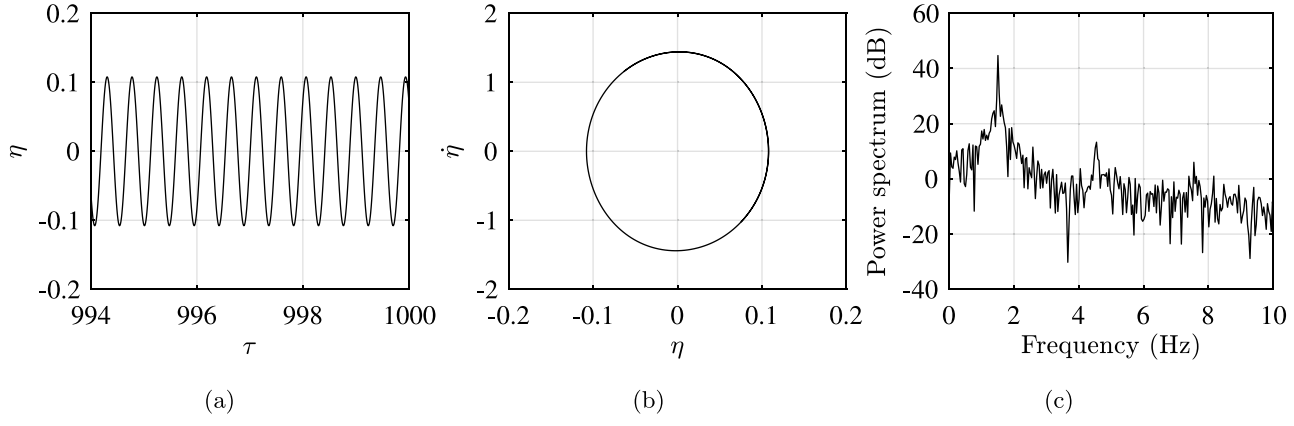

Fig. 7. (a) Time history plot, (b) phase-plane plot, and (c) power spectral density plot of Pipe 1 at $u_i = 6.57$ for $r_{ann} = 0.478$.

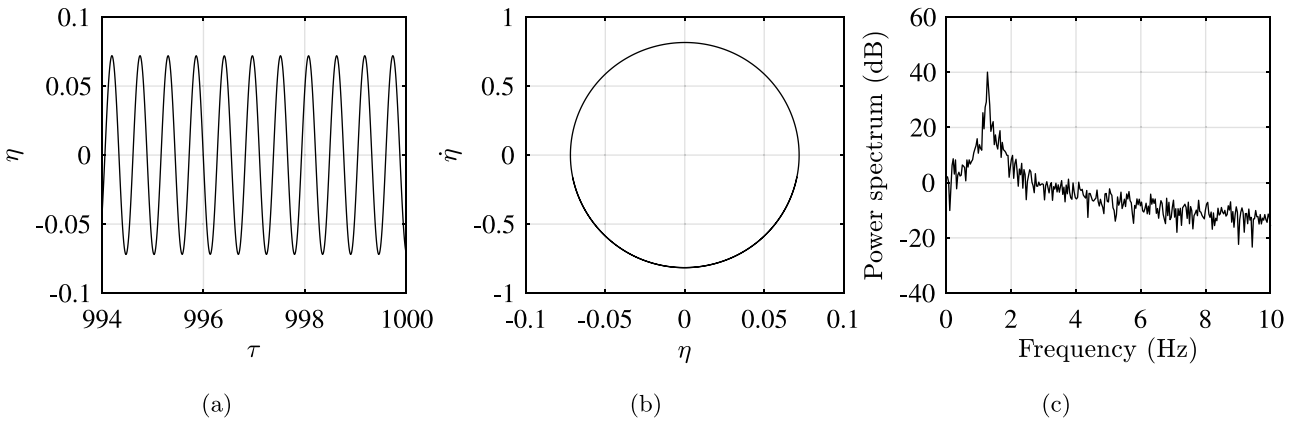

Fig. 8. (a) Time history plot, (b) phase-plane plot, and (c) power spectral density plot of Pipe 1 at $u_i = 6.51$ for $r_{ann} = 0.705$.

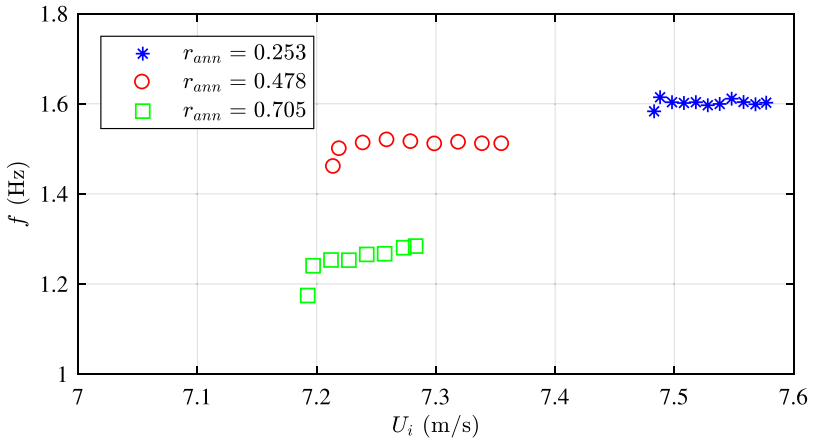

Fig. 9. Frequency of oscillations, f, in Hz, for Pipe 1 as a function of the dimensional internal flow velocity, U_i in m/s.

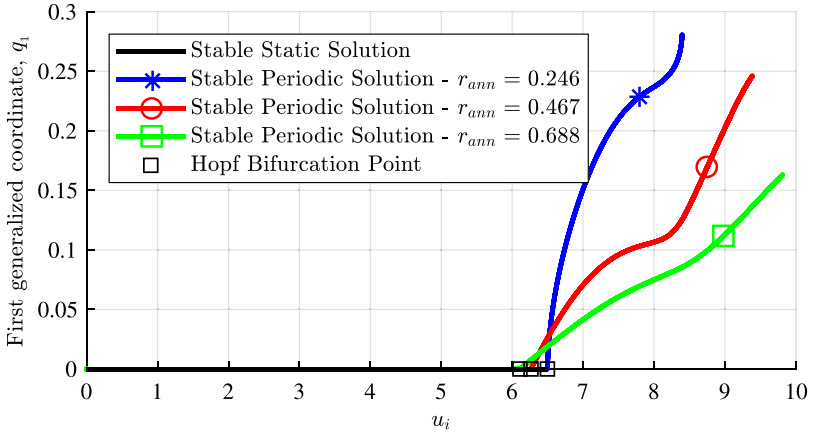

Fig. 10. Bifurcation diagrams for Pipe 2 with different lengths of the annular region showing the first generalized coordinate, q_1, as a function of the dimensionless internal flow velocity, u_i.

theoretical model [12] that both pipes lose stability at sufficiently high flow velocity via flutter in the second mode. The amplitude of oscillation recorded experimentally increases with increasing flow velocity, and eventually the pipes start hitting the rigid tube. These observations are in excellent qualitative agreement with the results of the present model.

The critical flow velocities for instability predicted by this model are summarized in Table 3, and they are compared to those reported in [12]. For Pipe 1, linear and nonlinear model predictions are quite similar.[5] Both models overestimate the values of u_{if} with respect to the experimental values. In contrast, for Pipe 2, both linear and nonlinear theories predict the onset of instability with 3% maximum difference with respect to the experimental data.

[5] It should be noted that the present model is identical to that in [12] in the linear limit, except that in the present study the viscous damping coefficient is given a constant value for each mode. This most likely is the reason for the small discrepancies.

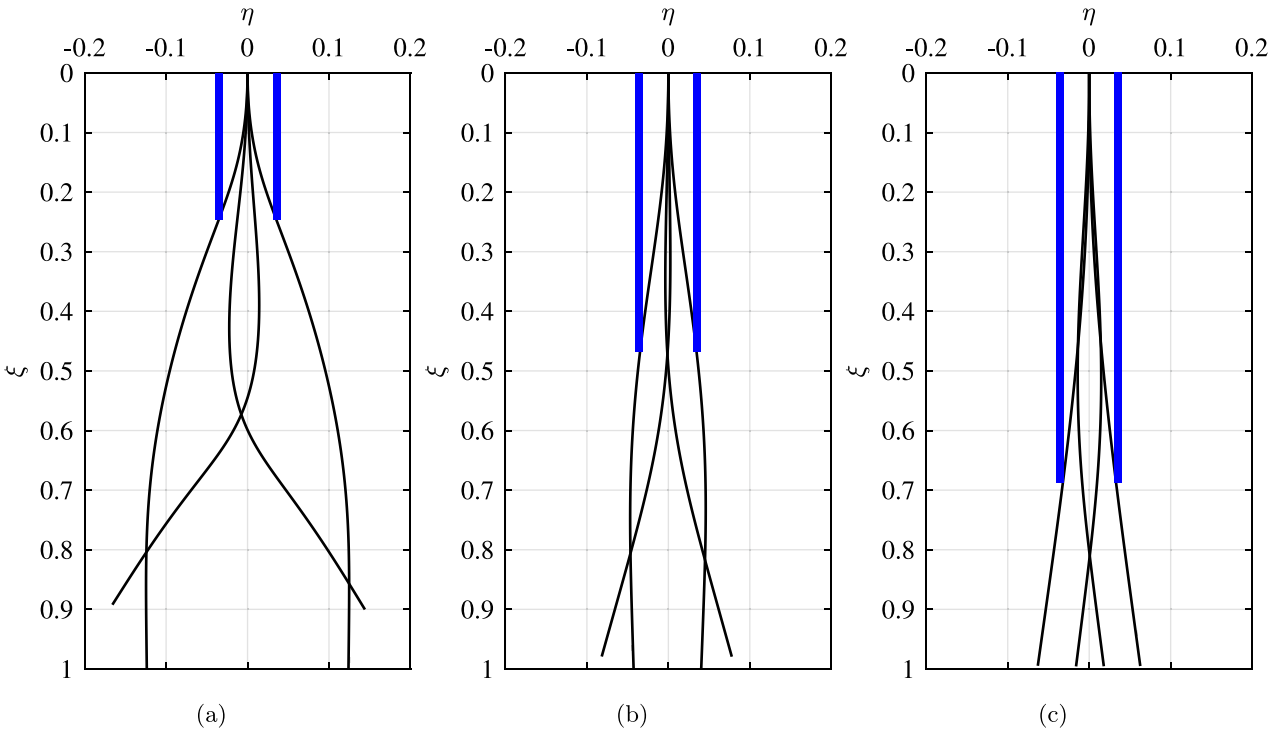

Fig. 11. Shapes of the oscillating Pipe 2 just before impacting the annulus-forming tube for: (a) r_{ann} = 0.246 at u_i = 6.80, (b) r_{ann} = 0.467 at u_i = 6.71, and (c) r_{ann} = 0.688 at u_i = 6.74.

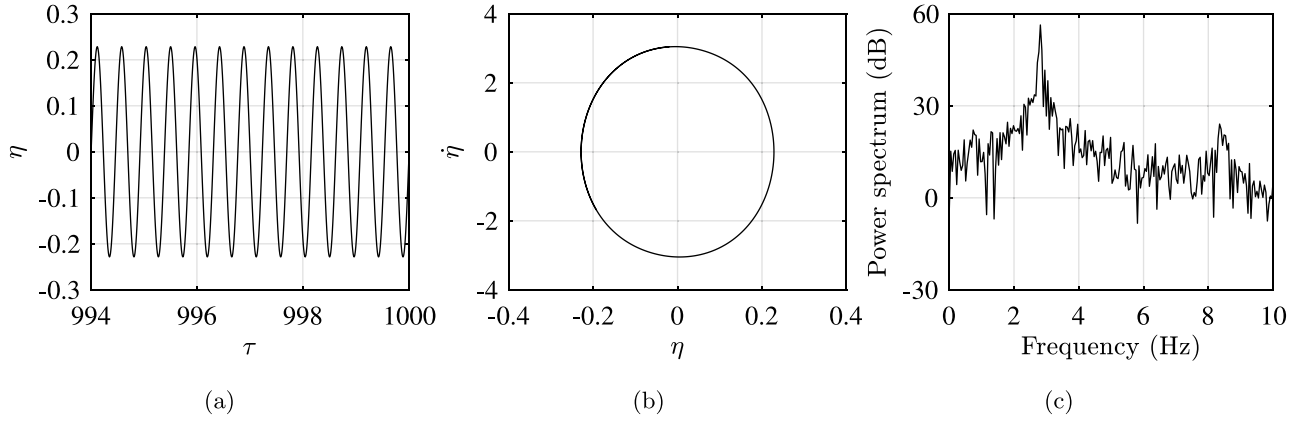

Fig. 12. (a) Time history plot, (b) phase-plane plot, and (c) power spectral density plot of Pipe 2 at u_i = 6.80 for r_{ann} = 0.246.

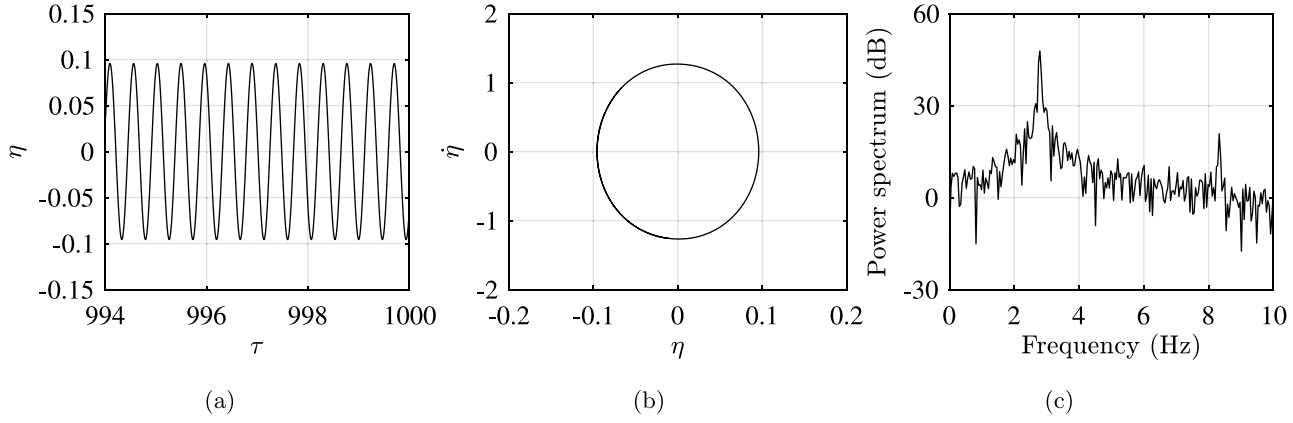

Fig. 13. (a) Time history plot, (b) phase-plane plot, and (c) power spectral density plot of Pipe 2 at u_i = 6.71 for r_{ann} = 0.467.

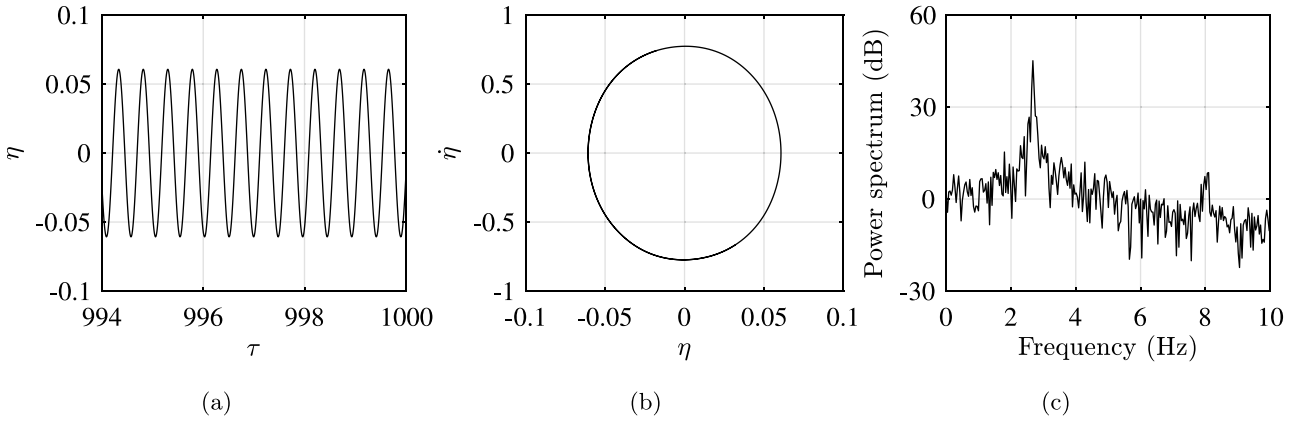

Fig. 14. (a) Time history plot, (b) phase-plane plot, and (c) power spectral density plot of Pipe 2 at $u_i = 6.74$ for $r_{ann} = 0.688$.

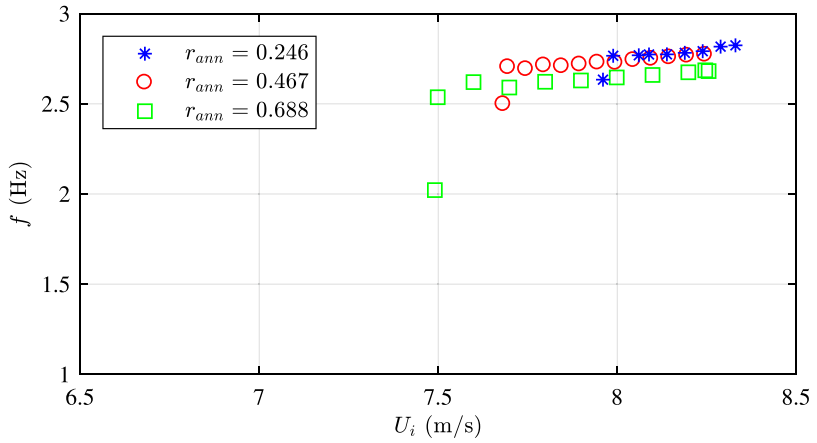

Fig. 15. Frequency of oscillations, f, in Hz, for Pipe 2 as a function of the dimensional internal flow velocity, U_i in m/s.

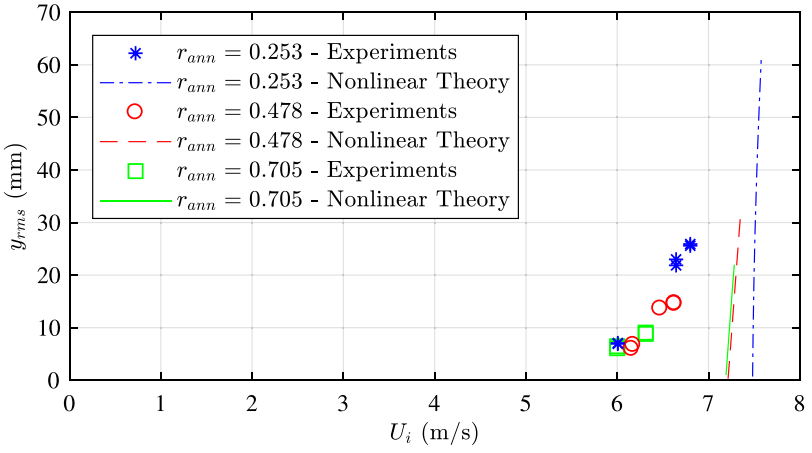

Fig. 16. Rms amplitude of oscillation, y_{rms}, for Pipe 1, 11 mm above the free end, as a function of the dimensional internal flow velocity, U_i.

The nonlinear theory can also predict additional quantitative facets of the dynamical behaviour of the system as compared to the linear one, such as limit-cycle amplitudes and frequencies. Figs. 16 and 17 show a comparison between the root-mean-square of the amplitudes of oscillation with increasing flow velocity for Pipes 1 and 2, respectively, obtained by the present model and those recorded experimentally by Moditis [36], for the experiments reported in [12]. All the results presented hereafter are calculated for a point very close to the free end of the pipe (11 mm above the free end), at the same location as the experimental data. It can be seen in Fig. 16 that the model can predict the amplitude of oscillation for Pipe 1 within a small range of flow velocities beyond the onset of instability — see Fig. 18 as well — considering the fact that the model overestimates that onset. However, the model also overestimates the amplitude of oscillations right before the pipe starts hitting the outer rigid tube, which is the maximum limit set in the figure. This may be partly due to the third-order approximation of the model. The uncertainty in the values given to the friction and form-drag coefficients, as well as the approximation made for the damping model, could also have contributed to the discrepancy. Almost the same comments apply to Fig. 17 (Pipe

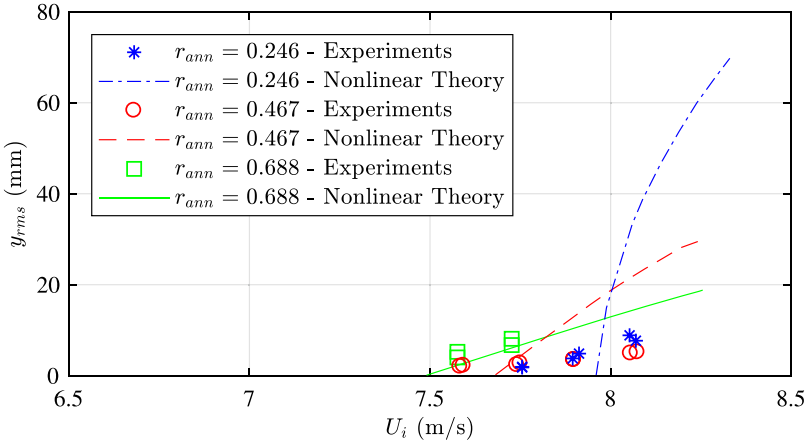

Fig. 17. Rms amplitude of oscillation, y_{rms}, for Pipe 2, 11 mm above the free end, as a function of the dimensional internal flow velocity, U_i.

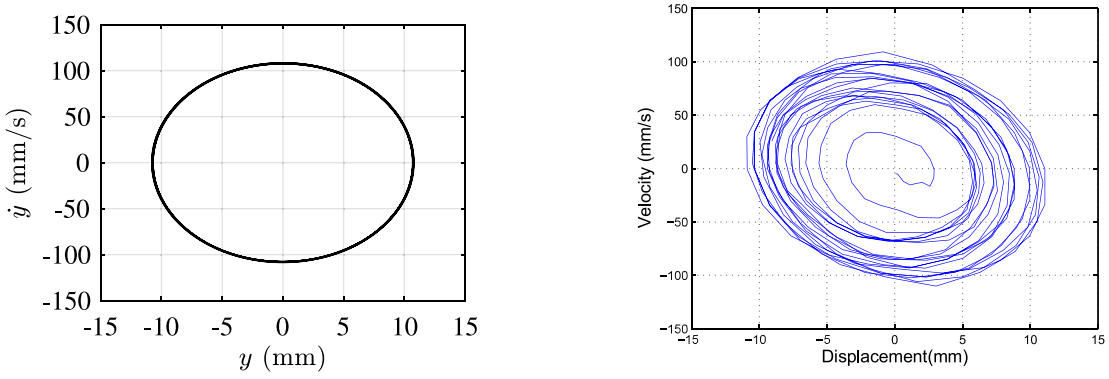

Fig. 18. Phase-plane plots for Pipe 1 with $r_{ann} = 0.253$, 11 mm above the free end, obtained by (a) the present nonlinear model at $U_i = 7.49$ m/s, and (b) experiments in [36] at $U_i = 6.00$ m/s.

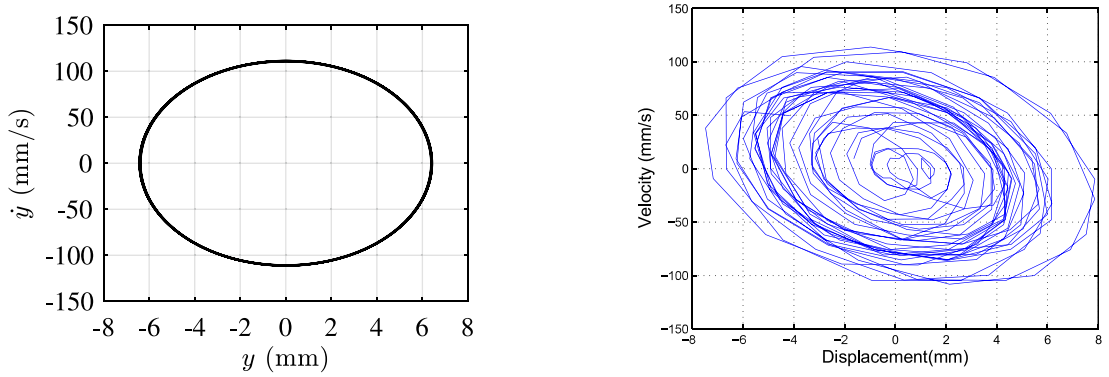

Fig. 19. Phase-plane plots for Pipe 2 with $r_{ann} = 0.246$, 11 mm above the free end, obtained by (a) the present nonlinear model at $U_i = 7.97$ m/s, and (b) experiments in [36] at $U_i = 7.89$ m/s.

2); however, interestingly, the discrepancy between the amplitude of oscillation predicted theoretically and that recorded experimentally for the larger lengths of the annulus, in the case of Pipe 2, is significantly smaller.

Phase-plane plots obtained at flow velocities very close to the critical ones are compared to those acquired experimentally and reported in [36] for the two pipes in Figs. 18 and 19; the figures show almost identical displacement amplitudes and velocities. However, it is worth mentioning that the experimental time history [36] for Pipe 2 with $r_{ann} = 0.246$ displays an intermittent motion, which results in a more densely populated phase-plane plot in Fig. 19b than in Fig. 18b, making it more difficult to determine the limit cycle. The experiments in [36] were conducted using two cameras at 90° to each other. Almost identical phase-plane plots were reported for the front- and side-camera experimental time histories, which suggests a planar motion with slowly rotating plane, as discussed in [12,36]. This justifies

Table 3
Comparison between the critical flow velocities for instability, u_{if}, for Pipes 1 and 2 with various lengths of the annular region obtained by different studies.

Pipe	r_{ann}	Linear theory [12]	Nonlinear theory	Experiments [12]
1	0.253	6.69	6.69	5.12
	0.478	6.47	6.44	5.29
	0.705	6.44	6.42	5.05
2	0.246	6.44	6.49	6.29
	0.467	6.27	6.27	6.16
	0.688	6.15	6.11	6.03

Table 4
Comparison between the frequency of oscillations in Hz at the onset of flutter for Pipe 1 with various lengths of the annular region obtained by different studies.

Pipe	r_{ann}	Linear theory [12]	Nonlinear theory	Experiments [12]
1	0.253	1.60	1.58	1.57
	0.478	1.51	1.46	1.45
	0.705	1.22	1.17	1.13
2	0.246	2.78	2.63	2.63
	0.467	2.70	2.49	2.47
	0.688	2.58	2.02	2.03

the basic assumption made in the present model that motions are two-dimensional; nevertheless, it is recognized that to fully capture the motion a three-dimensional model is required.

The frequencies of oscillation obtained right after the initiation of limit-cycle oscillation are presented in Table 4 for the two pipes. The frequencies obtained by the present model are in excellent agreement with those observed experimentally, better than predictions by the linear theory, for both pipes and for the different lengths of the annular region.

4.2. Discussion on the effect of annulus length

We first consider the results obtained by both linear and nonlinear theory for Pipe 1 in Table 3, together with the modal shapes in Fig. 5. It is noticed that the three values of r_{ann} are roughly 0.25, 0.50 and 0.70, thus they are almost linearly related. The values of u_{if} in Table 3, on the other hand, decrease nonlinearly, with the increase from $r_{ann} \simeq 0.25$ to $r_{ann} \simeq 0.50$ being much larger percentage-wise than that for $r_{ann} \simeq 0.50$ to $r_{ann} \simeq 0.70$.[6] Referring now to Fig. 5 it is noticed that the modal antinode for $r_{ann} \simeq 0.25$ is outside the annulus, while for $r_{ann} \simeq 0.50$ it is just inside the annulus, and more definitely inside for $r_{ann} \simeq 0.70$.[7] Since the antinode is associated with the maximum disturbance to the flow if it is in the confined space of the annulus, rather than outside, this may well result in the nonlinear effect for u_{if} discussed above.

The same applies to Pipe 2 (refer to Table 3 and Fig. 11), although the nonlinearity in this case is weaker. In this connection, however, it must be remembered that D_o for this pipe is smaller that for Pipe 1, and hence the annulus is relatively wider.

In any case, the effect of increasing the length of the annulus involves the balance of two opposing trends: (i) there is annular flow over a larger portion of the pipe, which is destabilizing, and (ii) there is increased added mass, which is stabilizing.

5. Influence of varying the tightness of the outer rigid tube

In this section the influence of varying the tightness of the annular region surrounding the pipe is investigated theoretically; there are no experimental data to compare with. The inner diameter of the outer rigid tube, D_{ch}, is varied resulting in different values of α_{ch}, and also χ and h. The other parameters of the system are kept constant to isolate the effect of the parameter of interest. The critical flow velocities, u_{if}, for each pipe with different r_{ann} and α_{ch} are listed in Table 5.[8] It may be concluded that increasing α_{ch} has a stabilizing effect on the system, leading to higher values of u_{if}; this is due to the decrease in the external flow velocity with increasing D_{ch}. Interestingly, decreasing α_{ch} not only decreases u_{if}, but it causes both pipes to undergo flutter in the first mode instead of the second, for $r_{ann} \approx 0.70$. The same mode of instability was predicted in [5,7] for a pipe discharging fluid with an external flow that is confined over the whole length of the pipe.

Table 5
The onset of instability, u_{if}, for Pipes 1 and 2 for different $\alpha_{ch} = D_{ch}/D_o$ and different lengths of the annular region, $r_{ann} = L'/L$.

Pipe	α_{ch}	$r_{ann} \approx 0.25$	$r_{ann} \approx 0.47$	$r_{ann} \approx 0.70$
1	1.50	6.37	5.68	5.06[a]
	1.97	6.65	6.47	6.46
	2.50	6.71	6.61	6.64
2	1.50	5.30	3.78	3.27[a]
	3.31	6.53	6.35	6.24
	5.00	6.58	6.49	6.45

[a]Denotes that the predicted flutter is in the first mode of the pipe.

Figs. 20 and 21 show samples of the bifurcation diagrams obtained by the nonlinear model[9] for Pipes 1 and 2, respectively, with $r_{ann} \approx 0.47$ and using different values of α_{ch}. Increasing α_{ch} to higher values than the original ones (i.e. $\alpha_{ch} = 1.97$ for Pipe 1 and 3.31 for Pipe 2) does not affect the stability of the system as dramatically as compared to decreasing α_{ch}, especially for Pipe 2, for which the original value of α_{ch} is relatively higher. This effect is not unexpected, as the flow velocity in the annulus scales inversely as the square of the annular flow area.

It is also noted that the effect of r_{ann} on the stability is strongest in the case of $\alpha_{ch} = 1.50$ when the modal antinode of the pipe is well within the annulus (not shown here for brevity).

6. Conclusion

In this paper, a nonlinear equation of motion has been derived for a cantilevered pipe simultaneously subjected to internal and partially-confined external annular flows. The equation of motion is exact to third-order of magnitude, assuming the lateral and axial displacements to be of first- and second-order of magnitude, respectively. The extended Hamilton's principle was used to obtain the equation of motion with a separate derivation of the fluid-related forces associated with the external flow, as well as the non-conservative forces due to the discharging fluid at the free end of the pipe. This equation is probably not the definitive nonlinear equation of motion for this system, since it was not obtained by a unified treatment of the fluid mechanics.

Two long flexible pipes of different dimensions and materials were considered in this study. The stability of these systems has been investigated with increasing internal flow velocity, which also results in increasing the external flow velocity in the annulus, as they are related to each other by continuity. The proposed nonlinear model predicts that the pipes lose stability via flutter in the second mode at sufficiently high flow velocity. The amplitude of the oscillations increases with

[6] Calculations for $r_{ann} = 0$ to $r_{ann} = 1$ confirm this nonlinear effect.

[7] It should be recalled that the modal shapes involve a travelling wave component, which makes these statements less than absolutely definite; the antinode travels along the pipe, as seen in Figs. 5 and 11 (cf. Figs. 3.48 and 3.51 in [37] and Fig. 2.22 in [28]).

[8] The results shown in Table 5 are obtained using a linearized form of the model derived in the present study, utilizing a ten-mode Galerkin approximation. Hence, slight differences with respect to the predictions of the nonlinear model are seen in the table for the original systems, i.e. $\alpha_{ch} = 1.97$ for Pipe 1 and 3.31 for Pipe 2; however, the maximum difference is less than 3%.

[9] In terms of the critical flow velocities for the two pipes with $r_{ann} \approx 0.47$ and different α_{ch}, the maximum difference between the predictions of the nonlinear model and the linearized one shown in Table 5 was again less than 3%.

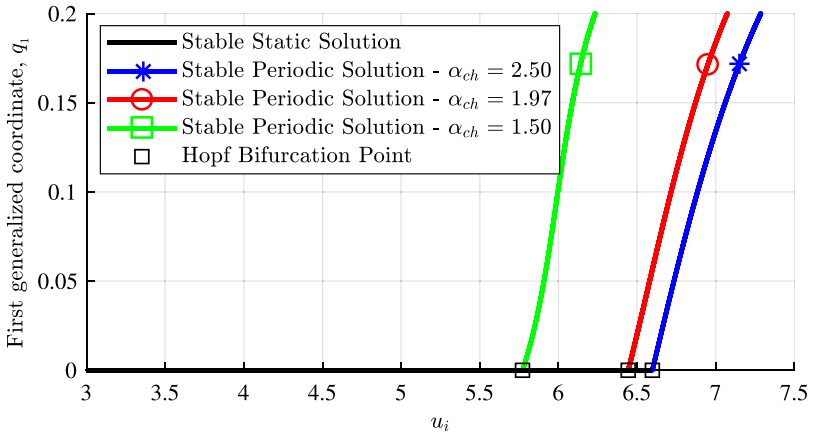

Fig. 20. Bifurcation diagrams for Pipe 1 with $r_{ann} = 0.478$ obtained for different values of α_{ch}.

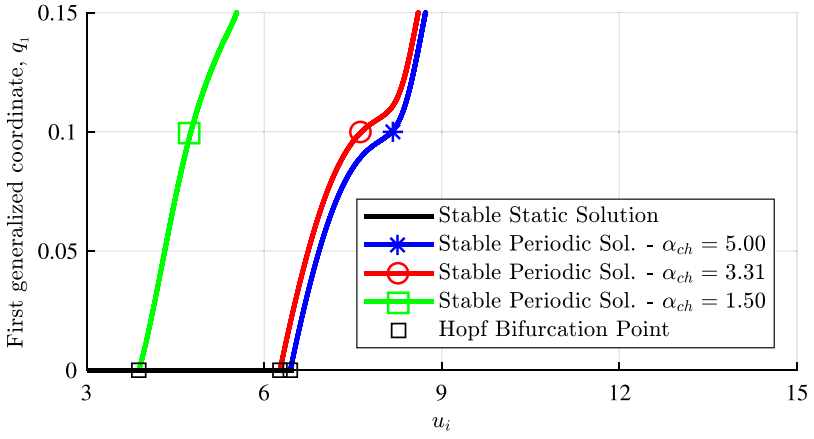

Fig. 21. Bifurcation diagrams for Pipe 2 with $r_{ann} = 0.467$ obtained for different values of α_{ch}.

increasing flow velocity and the pipes eventually impact the rigid tube forming the annulus. Quantitatively, the model overestimates the onset of instability for Pipe 1 with respect to experimental data available in the literature. However, excellent agreement with the experiments was found for Pipe 2, which is more slender and of smaller wall-thickness as compared to Pipe 1. In addition, other aspects of the predicted dynamical behaviour were compared to the experimental observations; generally, the model can predict the amplitude and frequency of oscillations right after the onset of instability accurately, but it overestimates the amplitude of the oscillations at higher flow velocities.

The influence of varying the length and tightness of the annular region was also investigated theoretically in this paper. It was shown that increasing the length of the annulus decreases the critical flow velocity of instability for both pipes, and it decreases the predicted amplitude and frequency of oscillation at high flow velocities. Increasing the tightness of the annular region by decreasing the inner diameter of the outer rigid tube also has a destabilizing effect and it can result in a first-mode rather than second-mode instability for sufficiently long annular regions.

Furthermore, it can be concluded that the performance of the present model is significantly better for higher lengths of the annular region. Excellent agreement between the amplitude of oscillations obtained by this model and recorded experimentally was found for Pipe 2, when the external flow is confined over 70% of the length of the pipe.

Acknowledgements

The financial support by the Natural Sciences and Engineering Research Council of Canada (NSERC), the Solution Mining Research Institute (SMRI), USA and Pipeline Research Council International (PRCI), USA is gratefully acknowledged. The first author is thankful to McGill University for a McGill Engineering Doctoral Award (MEDA). Also, the authors are grateful to the anonymous referee who made some insightful comments on the possible influence of the location of the modal antinode of the oscillating pipe, leading to the discussion now incorporated in Section 4.2 of the present paper.

Appendix

The nonlinear coefficients of the discretized equation of motion, i.e. Eq. (36), are given here, as follows:

$$r_{ijk} = \frac{1}{2}u_o^2 \varepsilon c_d \int_0^{r_{ann}} \phi_i \phi_j' |\phi_k'| \, \mathrm{d}\xi, \quad \bar{s}_{ijk} = \frac{1}{2}u_o \sqrt{\beta_o} \varepsilon c_d \int_0^{r_{ann}} \phi_i |\phi_j'| \phi_k \, \mathrm{d}\xi,$$

$$\tilde{s}_{ijk} = \frac{1}{2}u_o \sqrt{\beta_o} \varepsilon c_d \int_0^{r_{ann}} \phi_i \phi_j' |\phi_k| \, \mathrm{d}\xi, \quad t_{ijk} = \frac{1}{2}\beta_o \varepsilon c_d \int_0^{r_{ann}} \phi_i \phi_j |\phi_k| \, \mathrm{d}\xi,$$

$$\begin{aligned}\alpha_{ijkl} = {} & 2\chi u_o^2 \int_0^{r_{ann}} \phi_i \phi_j'' \phi_k' \phi_l' \, \mathrm{d}\xi + \frac{1}{4}u_o^2 \varepsilon(-c_N - c_T h) \int_0^{r_{ann}} \phi_i \phi_j' \phi_k' \phi_l' \, \mathrm{d}\xi \\ & + \frac{1}{2}\gamma \int_0^1 \phi_i \phi_j' \phi_k' \phi_l' \, \mathrm{d}\xi \\ & + \frac{3}{4}u_o^2 \varepsilon c_T (1+h) \int_0^{r_{ann}} (r_{ann} - \xi) \phi_i \phi_j' \phi_k' \phi_l'' \, \mathrm{d}\xi - \frac{3}{2}\gamma \\ & \times \int_0^1 (1-\xi) \phi_i \phi_j' \phi_k' \phi_l'' \, \mathrm{d}\xi \\ & + 4 \int_0^1 \phi_i \phi_j' \phi_k'' \phi_l''' \, \mathrm{d}\xi + \int_0^1 \phi_i \phi_j'' \phi_k'' \phi_l'' \, \mathrm{d}\xi + \int_0^1 \phi_i \phi_j'''' \phi_k' \phi_l' \, \mathrm{d}\xi\end{aligned}$$

$$
\begin{aligned}
&- \chi u_o^2 \int_0^1 \phi_i \phi_j'' \left(\int_\xi^{r_{ann}} \phi_k' \phi_l'' \, \mathrm{d}\xi \right) \mathrm{d}\xi - (1-\chi) u_o^2 \\
&\times \int_{r_{ann}}^1 \phi_i \phi_j'' \left(\int_\xi^{r_{ann}} \phi_k' \phi_l'' \, \mathrm{d}\xi \right) \mathrm{d}\xi \\
&- \Pi_{oL} \int_0^1 \phi_i \phi_j' \phi_k' \phi_l'' \, \mathrm{d}\xi + \Pi_{oL} \int_0^1 \phi_i \phi_j'' \left(\int_\xi^1 \phi_k' \phi_l'' \, \mathrm{d}\xi \right) \mathrm{d}\xi \\
&- \frac{1}{2} u_o^2 \varepsilon (c_T - c_N) \int_0^{r_{ann}} \phi_i \phi_j'' \left(\int_\xi^1 \phi_k' \phi_l' \, \mathrm{d}\xi \right) \mathrm{d}\xi \\
&+ u_i^2 \int_0^1 \phi_i \phi_j'' \phi_k' \phi_l' \, \mathrm{d}\xi - \frac{3}{2} (\Gamma - \Pi_{iL}) \int_0^1 \phi_i \phi_j' \phi_k' \phi_l'' \, \mathrm{d}\xi \\
&+ \frac{1}{2} (\Gamma - \Pi_{iL}) \int_0^1 \phi_i \phi_j'(1) \phi_k'(1) \phi_l'' \, \mathrm{d}\xi - u_i^2 \int_0^1 \phi_i \phi_j'' \\
&\times \left(\int_\xi^1 \phi_k' \phi_l'' \, \mathrm{d}\xi \right) \mathrm{d}\xi \\
&- \frac{1}{4} u_o^2 \varepsilon c_T h \int_0^1 \phi_i \phi_j'' \left\{ \int_\xi^1 \phi_k' \phi_l' [(r_{ann} - \xi) \delta_D(\xi - r_{ann}) \right. \\
&\left. - \mathrm{H}(\xi - r_{ann})] \, \mathrm{d}\xi \right\} \mathrm{d}\xi \\
&- \frac{1}{2} u_o^2 (1 + K_1) \int_0^1 \phi_i \phi_j'' \left(\int_\xi^1 \phi_k' \phi_l'' \, \mathrm{d}\xi \right) \mathrm{d}\xi + \frac{1}{4} u_o^2 K_1 \\
&\times \int_0^{r_{ann}} \phi_i \phi_j' \phi_k' \phi_l'' \, \mathrm{d}\xi,
\end{aligned}
$$

$$
\begin{aligned}
\beta_{ijkl} = {} & \chi u_o \sqrt{\beta_o} \left\{ \frac{1}{2} \int_0^{r_{ann}} \phi_i \phi_j' \phi_k' \phi_l' \, \mathrm{d}\xi + \frac{3}{2} \int_0^{r_{ann}} \phi_i \phi_j'' \phi_k' \phi_l \, \mathrm{d}\xi \right. \\
&\left. + 2 \int_0^1 \phi_i \phi_j'' \left(\int_\xi^{r_{ann}} \phi_k' \phi_l' \, \mathrm{d}\xi \right) \mathrm{d}\xi \right\} \\
&+ 2(1-\chi) u_o \sqrt{\beta_o} \int_{r_{ann}}^1 \phi_i \phi_j'' \left(\int_\xi^{r_{ann}} \phi_k' \phi_l' \, \mathrm{d}\xi \right) \mathrm{d}\xi \\
&- 2\chi u_o \sqrt{\beta_o} \int_0^{r_{ann}} \phi_i \phi_j'' \left(\int_0^\xi \phi_k' \phi_l' \, \mathrm{d}\xi \right) \mathrm{d}\xi \\
&- \frac{1}{4} u_o \sqrt{\beta_o} \varepsilon c_N \int_0^{r_{ann}} \phi_i \phi_j' \phi_k' \phi_l \, \mathrm{d}\xi + \frac{1}{2} u_o \sqrt{\beta_o} \varepsilon (c_T - c_N) \\
&\times \int_0^{r_{ann}} \phi_i \phi_j'' \left(\int_\xi^{r_{ann}} \phi_k' \phi_l \, \mathrm{d}\xi \right) \mathrm{d}\xi \\
&- 3\chi u_o \sqrt{\beta_o} \int_0^{r_{ann}} \phi_i \phi_j' \left(\int_0^\xi \phi_k' \phi_l'' \, \mathrm{d}\xi \right) \mathrm{d}\xi - 3\chi u_o \sqrt{\beta_o} \int_0^{r_{ann}} \phi_i \phi_j' \\
&\times \left(\int_0^\xi \phi_k'' \phi_l' \, \mathrm{d}\xi \right) \mathrm{d}\xi \\
&+ 2u_i \sqrt{\beta_i} \int_0^1 \phi_i \phi_j' \phi_k' \phi_l' \, \mathrm{d}\xi - 2u_i \sqrt{\beta_i} \int_0^1 \phi_i \phi_j'' \left(\int_\xi^1 \phi_k' \phi_l' \, \mathrm{d}\xi \right) \mathrm{d}\xi,
\end{aligned}
$$

$$
\begin{aligned}
\gamma_{ijkl} = {} & - \frac{3}{2} \chi \beta_o \int_0^1 \phi_i \phi_j' \phi_k \phi_l' \, \mathrm{d}\xi - \frac{3}{2} (1-\chi) \beta_o \int_{r_{ann}}^1 \phi_i \phi_j' \phi_k \phi_l' \, \mathrm{d}\xi + 2\chi \beta_o \\
&\times \int_0^1 \phi_i \phi_k' \left(\int_0^\xi \phi_j' \phi_l' \right) \mathrm{d}\xi \\
&+ 2(1-\chi) \beta_o \int_{r_{ann}}^1 \phi_i \phi_k' \left(\int_0^\xi \phi_j' \phi_l' \, \mathrm{d}\xi \right) \mathrm{d}\xi - (1-\beta_o) \int_0^1 \phi_i \phi_j'' \\
&\times \left(\int_\xi^1 \int_0^\xi \phi_k' \phi_l' \, \mathrm{d}\xi \, \mathrm{d}\xi \right) \mathrm{d}\xi \\
&+ \int_0^1 \phi_i \phi_j' \left(\int_0^\xi \phi_k' \phi_l' \, \mathrm{d}\xi \right) \mathrm{d}\xi + (\chi - 1) \beta_o \int_0^{r_{ann}} \phi_i \phi_j' \\
&\times \left(\int_0^\xi \phi_k' \phi_l' \, \mathrm{d}\xi \right) \mathrm{d}\xi \\
&+ \frac{1}{2} \beta_o \varepsilon c_N \int_0^1 \phi_i \phi_k \left(\int_0^\xi \phi_j' \phi_l' \, \mathrm{d}\xi \right) \mathrm{d}\xi + \frac{1}{4} \beta_o \varepsilon c_N \\
&\times \int_0^{r_{ann}} \phi_i \phi_j' \phi_k \phi_l \, \mathrm{d}\xi \\
&- \frac{1}{4} \beta_o \varepsilon c_T \int_0^1 \phi_i \phi_j'' \left(\int_\xi^1 \phi_k \phi_l \, \mathrm{d}\xi \right) \mathrm{d}\xi,
\end{aligned}
$$

$$
\eta_{ijkl} = - \frac{1}{4} \frac{\beta_o^{3/2} \varepsilon c_N}{u_o} \int_0^{r_{ann}} \phi_i \phi_j \phi_k \phi_l \, \mathrm{d}\xi,
$$

$$
\begin{aligned}
\mu_{ijkl} = {} & - (1-\beta_o) \int_0^1 \phi_i \phi_j'' \left(\int_\xi^1 \int_0^\xi \phi_k' \phi_l' \, \mathrm{d}\xi \, \mathrm{d}\xi \right) \mathrm{d}\xi - \chi \beta_o \\
&\times \int_0^1 \phi_i \phi_j'' \left(\int_\xi^1 \phi_k' \phi_l \, \mathrm{d}\xi \right) \mathrm{d}\xi \\
&- (1-\chi) \beta_o \int_{r_{ann}}^1 \phi_i \phi_j'' \left(\int_\xi^1 \phi_k' \phi_l \, \mathrm{d}\xi \right) \mathrm{d}\xi + \beta_o (\chi - 1) \\
&\times \int_0^{r_{ann}} \phi_i \phi_j' \left(\int_0^\xi \phi_k' \phi_l' \, \mathrm{d}\xi \right) \mathrm{d}\xi \\
&+ \int_0^1 \phi_i \phi_j' \left(\int_0^\xi \phi_k' \phi_l' \, \mathrm{d}\xi \right) \mathrm{d}\xi.
\end{aligned}
$$

References

[1] F. Cesari, S. Curioni, Buckling instability in tubes subject to internal and external axial fluid flow, in: Proceedings of the 4th Conference on Dimensioning, Hungarian Academy of Science, Budapest, 1971, pp. 301–311.

[2] M.J. Hannoyer, M.P. Païdoussis, Instabilities of tubular beams simultaneously subjected to internal and external axial flows, J. Mech. Des. 100 (2) (1978) 328–336.

[3] M.P. Païdoussis, P. Besançon, Dynamics of arrays of cylinders with internal and external axial flow, J. Sound Vib. 76 (3) (1981) 361–379.

[4] X. Wang, F. Bloom, Dynamics of a submerged and inclined concentric pipe system with internal and external flows, J. Fluids Struct. 13 (4) (1999) 443–460.

[5] M.P. Païdoussis, T.P. Luu, S. Prabhakar, Dynamics of a long tubular cantilever conveying fluid downwards, which then flows upwards around the cantilever as a confined annular flow, J. Fluids Struct. 24 (1) (2008) 111–128.

[6] A.R. Abdelbaki, A.K. Misra, M.P. Païdoussis, Nonlinear dynamics of a hanging cantilevered pipe simultaneously subjected to internal and external axial flows, in: the 9th international symposium on fluid-structure interactions, flow-sound interactions, flow-induced vibration and noise, paper fiv2018-138, 2018.

[7] A.R. Abdelbaki, M.P. Païdoussis, A.K. Misra, A nonlinear model for a hanging tubular cantilever simultaneously subjected to internal and confined external axial flows, J. Sound Vib. 449 (2019) 349–367.

[8] S. Rinaldi, Experiments on the Dynamics of Cantilevered Pipes Subjected to Internal and/or External Axial Flow (Master of Engineering Thesis), Department of Mechanical Engineering, McGill University, 2009.

[9] Q. Qian, L. Wang, Q. Ni, Vibration and stability of vertical upward-fluid-conveying pipe immersed in rigid cylindrical channel, Acta Mech. Solida Sin. 21 (5) (2008) 331–340.

[10] K. Fujita, A. Moriasa, Stability of cantilevered pipes subjected to internal flow and external annular axial flow simultaneously, in: ASME 2015 Pressure Vessels and Piping Conference, American Society of Mechanical Engineers, Paper V004T04A020, 2015.

[11] G.-H. Zhao, S. Tang, Z. Liang, J. Li, Dynamic stability of a stepped drillstring conveying drilling fluid, J. Theoret. Appl. Mech. 55 (4) (2017) 1409–1422.

[12] K. Moditis, M.P. Païdoussis, J. Ratigan, Dynamics of a partially confined, discharging, cantilever pipe with reverse external flow, J. Fluids Struct. 63 (2016) 120–139.

[13] J.L. Ratigan, Underground storage of hydrocarbons in salt formations, in: Operating Section Proceedings - American Gas Association, Las Vegas, NY, USA, pp. 710–718, Paper 95-OP-20, 1995.

[14] K. Kontzialis, K. Moditis, M.P. Païdoussis, Transient simulations of the fluid–structure interaction response of a partially confined pipe under axial flows in opposite directions, J. Press. Vessel Technol. 139 (3) (2017) 031303.

[15] S. Minas, M.P. Païdoussis, F. Daneshmand, Experimental and analytical investigation of hanging tubular cantilevers with discharging axial and radial flow, in: ASME 2017 International Mechanical Engineering Congress and Exposition, American Society of Mechanical Engineers, Paper V04AT05A037, 2017.

[16] S. Rinaldi, M.P. Païdoussis, Dynamics of a cantilevered pipe discharging fluid, fitted with a stabilizing end-piece, J. Fluids Struct. 26 (3) (2010) 517–525.

[17] A.R. Abdelbaki, A.K. Misra, M.P. Païdoussis, Dynamics of a tubular cantilever simultaneously subjected to internal and partially-confined external axial flows, in: ASME 2018 International Design Engineering Technical Conferences and Computers and Information in Engineering Conference, American Society of Mechanical Engineers, Paper V006T09A025, 2018.

[18] C. Semler, G.X. Li, M.P. Païdoussis, The non-linear equations of motion of pipes conveying fluid, J. Sound Vib. 169 (5) (1994) 577–599.

[19] J.L. Lopes, M.P. Païdoussis, C. Semler, Linear and nonlinear dynamics of cantilevered cylinders in axial flow. Part 2: The equations of motion, J. Fluids Struct. 16 (6) (2002) 715–737.

[20] T.B. Benjamin, Dynamics of a system of articulated pipes conveying fluid-i. theory, Phil. Trans. R. Soc. A 261 (1307) (1962) 457–486.

[21] E.F. Brater, H.W. King, J.E. Lindell, C. Wei, Handbook of Hydraulics for the Solution of Hydraulic Engineering Problems, Vol. 7, McGraw-Hill New York, 1976.
[22] M.P. Païdoussis, Dynamics of flexible slender cylinders in axial flow. Part 1. Theory, J. Fluid Mech. 26 (1966) 717–736.
[23] M.P. Païdoussis, Dynamics of flexible slender cylinders in axial flow. Part 2. Experiments, J. Fluid Mech. 26 (1966) 737–751.
[24] M.P. Païdoussis, Dynamics of cylindrical structures subjected to axial flow, J. Sound Vib. 29 (3) (1973) 365–385.
[25] M.P. Païdoussis, E. Grinevich, D. Adamovic, C. Semler, Linear and nonlinear dynamics of cantilevered cylinders in axial flow. Part 1: Physical dynamics, J. Fluids Struct. 16 (6) (2002) 691–713.
[26] A.R. Abdelbaki, M.P. Païdoussis, A.K. Misra, A nonlinear model for a free-clamped cylinder subjected to confined axial flow, J. Fluids Struct. 80 (2018) 390–404.
[27] M.J. Lighthill, Note on the swimming of slender fish, J. Fluid Mech. 9 (2) (1960) 305–317.
[28] M.P. Païdoussis, Fluid-Structure Interactions: Slender Structures and Axial Flow, Vol. 2, second ed., Academic Press, 2016.
[29] G.I. Taylor, Analysis of the swimming of long and narrow animals, Phil. Trans. R. Soc. A 214 (1117) (1952) 158–183.
[30] W. Bollay, A non-linear wing theory and its application to rectangular wings of small aspect ratio, ZAMM-J. Appl. Math. Mech./Z. Angew. Math. Mech. 19 (1) (1939) 21–35.
[31] G.S. Triantafyllou, C. Chryssostomidis, The dynamics of towed arrays, ASME J. Offshore Mech. Arct. Eng. 111 (3) (1989) 208–213.
[32] V.F. Sinyavskii, V.S. Fedotovskii, A.B. Kukhtin, Oscillation of a cylinder in a viscous liquid, Int. Appl. Mech. 16 (1) (1980) 46–50.
[33] S.S. Chen, M.W. Wambsganss, J.A. Jendrzejczyk, Added mass and damping of a vibrating rod in confined viscous fluids, J. Appl. Mech. 43 (2) (1976) 325–329.
[34] M.P. Païdoussis, N.T. Issid, Dynamic stability of pipes conveying fluid, J. Sound Vib. 33 (3) (1974) 267–294.
[35] E.J. Doedel, B.E. Oldeman, A.R. Champneys, F. Dercole, T.F. Fairgrieve, Y.A. Kuznetsov, R. Paffenroth, B. Sandstede, X. Wang, C. Zhang, AUTO-07P: Continuation and bifurcation software for ordinary differential equations (procurable from doedel@cs.concorida.ca), 2012.
[36] K. Moditis, The Dynamics of Hanging Tubular Cantilevers in Axial Flow: An Experimental and Theoretical Investigation (Master of Engineering Thesis), Department of Mechanical Engineering, McGill University, 2015.
[37] M.P. Païdoussis, Fluid-Structure Interactions: Slender Structures and Axial Flow, Vol. 1, second ed., Academic Press, 2014.